Naval Oceanographic Office

Stennis Space Center
MS 39522-5001

Technical Report
TR 311
August 1993

TR 311

INITIAL ANALYSIS AND MODELING RESULTS FROM THE POLAR ORBITING GEOMAGNETIC SURVEY (POGS) SATELLITE

Prepared under the authority of
Commander,
Naval Oceanography Command

FOREWORD

Global, regional, and local models of the Earth's magnetic field have a wide range of military applications both in the traditional sense as aids to navigation and attitude/heading reference systems (AHRS) for aircraft, missiles, tanks, ships, and remotely piloted/operated vehicles (RPV/ROV) and in the modern sense as tools of analysis with respect to submarine and subterranean detection/concealment, electronic jamming, endoatmospheric charge particle beam weaponry, and the monitoring of nuclear test sites. Beyond military issues, these models also have extensive scientific applications. Global magnetic field models for instance are used as boundary conditions at the core-mantle interface to evaluate competing theories of the Earth's magnetohydrodynamic dynamo. Regional and local field models are used for mineral resource evaluation and are critical to the understanding of the geological history of the Earth's crust.

These models are phenomenological in origin, which means that they require survey data to support them. Furthermore, since the Earth's Main (Core-generated) magnetic field varies slowly but erratically with time, it is necessary to perform global resurveys of this field at least periodically, if not continuously. Low-altitude, polar orbiting satellite platforms provide the most efficient means of achieving the required spatial uniformity of coverage and corresponding temporal cohesiveness.

The Polar Orbiting Geomagnetic Survey (POGS) satellite represents the Navy's continuing effort, as part of the Project MAGNET program, which was established at the Naval Oceanographic Office in 1951, to secure the necessary data to maintain accurate magnetic field models to support all validated DOD requirements for these models. In particular, this data is intended to support the 1995 Epoch World Magnetic Model (WMM-95). At the same time, the value of this data for scientific purposes is fully recognized. Consequently, as with all other high-altitude Project MAGNET aircraft data intended for use in the World Magnetic Modeling (WMM) program, POGS data is routinely being made available to the general public through the National Geophysical Data Center, Boulder, CO.

T.E. CALLAHAM
Captain, U.S. Navy
Commanding Officer

DISCLAIMER NOTICE

THIS DOCUMENT IS BEST QUALITY AVAILABLE. THE COPY FURNISHED TO DTIC CONTAINED A SIGNIFICANT NUMBER OF COLOR PAGES WHICH DO NOT REPRODUCE LEGIBLY ON BLACK AND WHITE MICROFICHE.

REPORT DOCUMENTATION PAGE

Form Approved
OMB No. 0704-0188

1. AGENCY USE ONLY (Leave blank)	2. REPORT DATE	3. REPORT TYPE AND DATES COVERED
	August 1993	Technical Report

4. TITLE AND SUBTITLE

INITIAL ANALYSIS AND MODELING RESULTS FROM THE POLAR ORBITING GEOMAGNETIC SURVEY (POGS) SATELLITE

5. FUNDING NUMBERS

6. AUTHOR(S)

John M. Quinn, Donald L. Shiel,
Mario H. Acuna, and John Scheifle

7. PERFORMING ORGANIZATION NAME(S) AND ADDRESS(ES)

Commanding Officer
Naval Oceanographic Office
1002 Balch Blvd.
Stennis Space Center, MS 39522-5001

8. PERFORMING ORGANIZATION REPORT NUMBER

TR 311

9. SPONSORING/MONITORING AGENCY NAME(S) AND ADDRESS(ES)

Commander
Naval Oceanography Command
1020 Balch Blvd.
Stennis Space Center, MS 39529-5005

10. SPONSORING/MONITORING AGENCY REPORT NUMBER

11. SUPPLEMENTARY NOTES

Prepared in cooperation with the National Aeronautics and Space Administration, Goddard Space Flight Center, Greenbelt, MD.

12a. DISTRIBUTION/AVAILABILITY STATEMENT

Approved for public release;
distribution in unlimited.

12b. DISTRIBUTION CODE

13. ABSTRACT (Maximum 200 words)

The spatial and temporal character of fully calibrated geomagnetic data collected on selected orbits of the Polar Orbiting Geomagnetic Survey (POGS) satellite mission during the first 6 months of 1991 is analyzed with respect to a preliminary, degree 12 spherical-harmonic magnetic field model derived from selected POGS data collected during January and February 1991. The accuracy of global models derived from these data depends on the vector magnetometer calibrations, thermal corrections, satellite magnetic mapping, and the time syncing of the satellite's quartz clock with respect to the satellite's ephemeris, which is referenced to Universal Time (UT) and which is supplied by the Defense Mapping Agency's tracking network (TRANET). The calibration and correction factors applied to the POGS data set are fully documented. Additionally, the current status of the POGS satellite and the corresponding data reduction and distribution efforts along with the current status of subsequent POGS experiments, which are part of the Defense Meteorological Satellite Program (DMSP) Block 5 and Block 6 satellite missions known as DMSP/POGS follow-on experiments, are presented.

14. SUBJECT TERMS	15. NUMBER OF PAGES
Magnetic field models, local field models, POGS satellite, Project MAGNET, Defense Meteorological Satellite Program (DMSP)	66
	16. PRICE CODE

17. SECURITY CLASSIFICATION OF REPORT	18. SECURITY CLASSIFICATION OF THIS PAGE	19. SECURITY CLASSIFICATION OF ABSTRACT	20. LIMITATION OF ABSTRACT
UNCLASSIFIED	UNCLASSIFIED	UNCLASSIFIED	UL

INITIAL ANALYSIS AND MODELING RESULTS FROM THE POLAR ORBITING GEOMAGNETIC SURVEY (POGS) SATELLITE

John M. Quinn and Donald L. Shiel
Naval Oceanographic Office
Stennis Space Center, MS 39522-5001

and

Mario H. Acuna and John Scheifle
National Aeronautics and Space Administration
Goddard Space Flight Center
Greenbelt, MD 20771

TABLE OF CONTENTS

List of Figures

List of Tables

1. INTRODUCTION

The U. S. Navy's Polar Orbiting Geomagnetic Survey (POGS) satellite was launched 11 April 1990. This launch culminated the efforts of several government agencies and private contractors. Principle among these were the Naval Oceanographic Office (NAVOCEANO); the Commander, Naval Oceanography Command (COMNAVOCEANCOM); the Defense Mapping Agency (DMA); the Air Force Space Test Program (STP); the Navy Space Systems Activity (NSSA); the Office of Naval Research (ONR); the National Aeronautics and Space Administration (NASA); and Defense Systems Incorporated (DSI). The POGS program is sponsored by COMNAVOCEANCOM, which falls under the auspices of the Oceanographer of the Navy (N096). It is NAVOCEANO's responsibility to operate the satellite and the ground stations which collect the POGS data, while it is DMA's responsibility to track the satellite, using its global tracking network (TRANET), and to provide the satellite ephemeris which NAVOCEANO merges with the POGS data. The integration of the POGS experiment with the Atlas launch vehicle and the coordination with the DSI contractors that built the satellite were the responsibility of STP, with the assistance of NSSA and ONR. The experiment vector magnetometer was built by NASA and was calibrated and tested at NASA's Goddard Space Flight Center (GSFC), which operates NASA's Spacecraft Magnetic Test Facility. A report on this facility is provided by NASA/GSFC (1984).

The POGS satellite was launched into a circular, polar orbit as part of a multi-satellite project known as P-87 STACKSAT, which in addition to POGS included two communication satellites of similar exterior design as indicated in Figure 1. The POGS satellite, the design characteristics of which are listed in Table 1, is at the top of the stack. It has 52 solar panels, some of which are used as sun sensors to provide a rough estimate, within a few degrees, of the

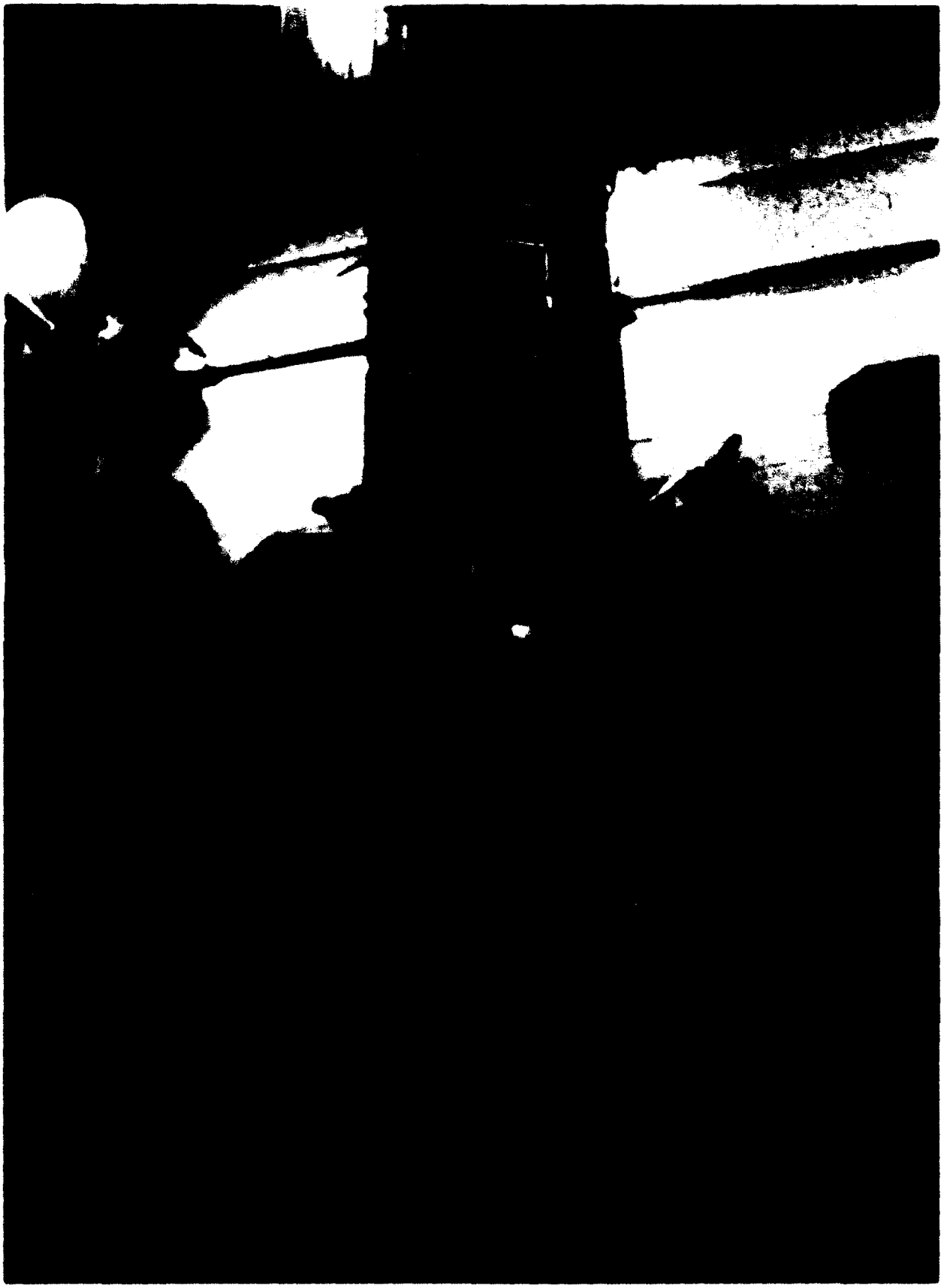

Figure 1. P-87 STACKSAT Prior to Final Assembly: POGS at the Top of the Stack

Table 1. POGS Design Characteristics

- **EXPERIMENT MAGNETOMETER**
  - **MODIFIED DMSP/SSM TRIAXIAL FLUXGATE (NASA)**
  - **RANGE: ± 65535 nT**
  - **RESOLUTION: ± 2 nT**
  - **LOCATION: AT TIP OF 8-FT Cu/Be (NON-MAGNETIC) BOOM**
- **ATTITUDE CONTROL**
  - **GRAVITY GRADIENT STABILIZATION**
    - **20-FT BOOM**
    - **5.12-LB TIP MASS**
  - **4 HYSTERESIS RODS**
  - **"Z" TORQUING COIL**
    - **45 AMP-TURN/METER**
    - **PERFORMS SATELLITE FLIP MANEUVERS**
- **ATTITUDE DETERMINATION**
  - **ONBOARD TRIAXIAL FLUXGATE MAGNETOMETER**
    - **RESOLUTION: ± 511 nT**
    - **LOCATION: ONBOARD SPACECRAFT**
  - **9 SUN SENSORS LOCATED AROUND SATELLITE**
    - **RESOLUTION: ± 3°**
    - **DETERMINES: AZIMUTH & ELEVATION (RELATIVE TO SUN-LINE)**
- **POSITIONING**
  - **RESOLUTION: 75 METERS SPHERICAL PROBABLE ERROR (SEP)**
  - **GRAVITY MODEL: GEM-10B**

satellite's attitude (i.e., azimuth and elevation relative to the Sun-line). The satellite is gravity-gradient stabilized and is tracked by a global network which monitors the satellite's two navigation beacons, which transmit signals at separate frequencies at 20-second intervals. The satellite carries two vector magnetometers, the coarse onboard Navigation magnetometer, which is used for attitude sensing of the satellite, and the high-resolution Experiment magnetometer, which is located at the tip of an 8-ft nonmagnetic boom. These are oriented relative to the earth and with respect to each other as indicated in Figure 2.

Four significant problems were encountered during the satellite's initial operations, all of which have been overcome. First, the satellite was launched into orbit in an inverted mode. There was a 50 percent probability that this would occur. As a consequence, the satellite's communications antennae pointed spaceward rather than earthward. This caused communication problems between the satellite and the ground stations. Although torquing coils were available to flip the satellite, this was considered a risky procedure which could have snapped the gravity-gradient boom or the Experiment magnetometer boom. Consequently, several months were spent redesigning the ground station antennae patterns. The Master ground station is located at Stennis Space Center, MS. A second ground station was operated by the U.S. Geological Survey through 1992. It was located at Fairbanks, AK. This ground station has since been replaced with another ground station operated by the U.S. Navy at Keflavik, Iceland. The communications problem was resolved by November 1990. A second problem concerned the satellite's onboard data packing and storage program. The Experiment magnetometer's data collection system was designed to store 1-second data samples in 10-second packets. The first record in each packet was a complete record, while the following nine records were 1-second delta values. Unfortunately, the program placed the Y-component deltas into both the

SENSOR COORDINATE SYSTEMS

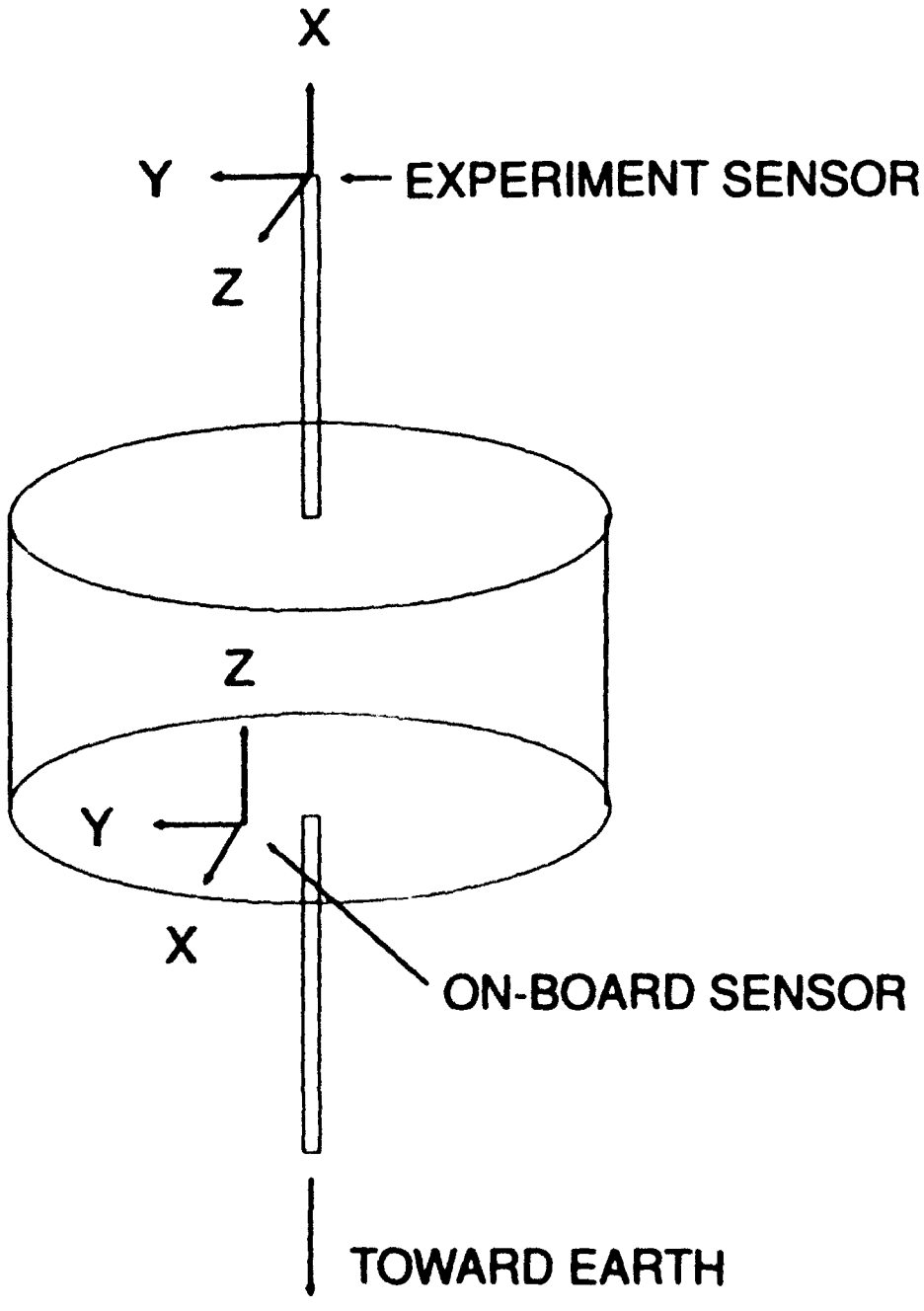

Figure 2. Relative Orientation of Magnetometer Coordinate Axes

Y-component and Z-component storage slots. This error was uncorrectable, resulting in an effective data sample rate of 10 samples per second instead of 1 sample per second. The third problem concerned the inability to monitor the drift of the satellite's onboard quartz clock via scheduled timing pulses. This problem was resolved by another modification to the ground station hardware in December 1990. As a result, useful POGS data begins in January of 1991. Satellite operations were continuous from that time (except for some minor down time due to radiation hits) until September 1992, when radiation caused the fourth problem, a disruption of that part of the satellite's memory which contained data downlink instructions. Communication with the satellite was lost for 5 months but was reestablished in January 1993. From that time forward the satellite has continued to operate normally. The satellite's orbit characteristics and other mission details are listed in Table 2.

2. MAGNETOMETER CALIBRATIONS

The Experiment magnetometer was calibrated at NASA/GSFC's Magnetic Coil Facility, where the magnetometer's scale factors, biases, orthogonality factors, and temperature characteristics were determined. Scale factors for the Navigation magnetometer were also determined at this facility. Some time later, when the Experiment magnetometer was attached to the satellite and the boom extended, a static magnetic-field measurement was performed to determine the satellite's magnetic signature at the site of the Experiment magnetometer. This test was performed with all satellite electronic packages turned on.

Table 2. POGS Mission Details

- **ORBITAL PARAMETERS**

- APPROXIMATE PERIOD:	98.61 Min
- SEMI-MAJOR AXIS:	7059.44 KM
- SEMI-MINOR AXIS:	7059.22 KM
- APOGEE RADIUS:	7115.95 KM
- PERIGEE RADIUS:	7002.94 KM
- INCLINATION:	89.88 Deg
- MEAN ALTITUDE:	688.33 KM

- **LAUNCH PARAMETERS**

- LAUNCH DATE:	11 APRIL 1990
- LAUNCH TIME:	0200 UT
- LAUNCH SITE:	VANDENBERG AFB, CALIFORNIA
- LAUNCH AZIMUTH:	180 Deg

- **MISSION OPERATIONS**

- MISSION LIFE EXPECTANCY:	1 TO 3 YEARS
- TRACKING ORGANIZATION:	DEFENSE MAPPING AGENCY
- TRACKING BEACON FREQUENCIES:	150/400 MHz
- DOWNLINK GROUND STATIONS:	NAVOCEANO, SSC, MS
	USGS, FAIRBANKS, AK
	U.S. NAVY, KEFLAVIK, ICELAND

2.1 The Navigation Magnetometer

The Navigation vector magnetometer is intended to measure the ambient magnetic field to a resolution of only $\pm$ 511 nanoTeslas (nT). The intended purpose of this magnetometer is to determine the satellite's orientation primarily just after orbit insertion and satellite spin-down. Each vector axis has its own scaling formula which converts from counts (i.e., relative voltage) to nanoTeslas. The dimensionless scale factors for the X-, Y-, and Z-axes of this magnetometer are:

$$S_x = 0.92761 \tag{1a}$$

$$S_y = 1.05508 \tag{1b}$$

$$S_z = 0.99245 \tag{1c}$$

With n_x , n_y , and n_z being the measured counts (range: 0 to 255) from the Navigation magnetometer, the magnetic field for this magnetometer is reconstructed for each vector axis in nanoTeslas as:

$$B_x = (n_x - 132)(60000.0/127)S_x \tag{2a}$$

$$B_y = (n_y - 129)(60000.0/127)S_y \tag{2b}$$

$$B_z = -(n_z - 130)(60000.0/127)S_z \tag{2c}$$

At the time that measurements are taken, the axes of the Navigation magnetometer (i.e., the onboard magnetometer) are oriented as indicated in Figure 2, which is a left-handed system.

The Navigation magnetometer's X- and Y-axes are parallel to the spacecraft coordinate axes, while the Z-axis is anti-parallel to the corresponding Z-axis of the spacecraft, which is the spin axis. The leading negative sign in eq. (2c) inverts the Z-axis of the Navigation magnetometer, thus making it parallel to the spacecraft coordinate Z-axis and in the process converts the left-handed Navigation magnetometer coordinate system into a right-handed coordinate system, with the Z-axis pointing toward the earth.

2.2 The Experiment Magnetometer

There are four aspects to the calibration of the high-resolution Experiment magnetometer. The first aspect is concerned with determining the calibration factors, which convert the sensor measurements from counts (essentially voltage measurements) to nanoTeslas. The second aspect is concerned with the precise determination of the orthogonality (i.e., alignment) of the vector axes of the Experiment magnetometer. The third factor involves the determination of the magnetic noise generated by the spacecraft and sensed by the Experiment magnetometer at the tip of the fully extended magnetometer boom, when all electronic packages are operating. The fourth factor is to determine the temperature sensitivity of the three axes of the Experiment magnetometer.

The Experiment magnetometer is of the same type that was designed and built by NASA for the Defense Meteorological Satellite Program (DMSP). The only modification in the design was to add extra thermal mass in order to reduce the magnetometer's thermal drift to something less than 50 nT/yr. The precise thermal drift is unknown. However, it is expected that this drift should be the greatest just after the satellite's initial insertion into orbit and that after a few days or weeks would settle down to a rather small value. There is no absolute scalar magnetometer to

monitor this drift rate and no other direct means to determine it. The initial analysis of the data after nearly a year in orbit indicates that the drift is much less than 50 nT/yr, when compared to predictions of 1990 Epoch spherical-harmonic magnetic field models that were generated from data independent of POGS.

The calibration constants for the POGS Experiment magnetometer are given in Table 3. The "measured" magnetic field vector components based on these calibration constants are computed according to the following formulae:

$$B_x = a_{x0} + \sum_{n=1}^{5} a_{xn} b_{xn(\text{coarse})} + K_x (b_{x(\text{fine})} - b_{x0}) \tag{3a}$$

$$B_y = a_{y0} + \sum_{n=1}^{5} a_{yn} b_{yn(\text{coarse})} + K_y (b_{y(\text{fine})} - b_{y0}) \tag{3b}$$

$$B_z = -\left[a_{z0} + \sum_{n=1}^{5} a_{zn} b_{zn(\text{coarse})} + K_z (b_{z(\text{fine})} - b_{z0}) \right] \tag{3c}$$

The factors $b_{x(\text{coarse})}$, $b_{y(\text{coarse})}$, and $b_{z(\text{coarse})}$ are the COARSE bias step intervals of the measured magnetic field, while factors $b_{x(\text{fine})}$, $b_{y(\text{fine})}$, and $b_{z(\text{fine})}$ are the FINE adjustments of the measured magnetic field. The division of the magnetic field measurements into COARSE and FINE segments is related to the compact, binary-packing scheme used to compress and store the data. Notice again that in the reconstruction of the magnetic field vector components a coordinate transformation must also been performed. As indicated in Figure 2, the X-axis of the Experiment magnetometer (Experiment sensor) is aligned along the spin axis of the satellite, while the Z-axis of this magnetometer is in the X-Y plane of the spacecraft's coordinate system.

Table 3. POGS Experiment Magnetometer Calibration Constants

CONSTANT \ COMPONENT	X-AXIS	Y-AXIS	Z-AXIS
K [nT/count]	1.998240	1.998800	1.998344
a_0 [nT]	-66385.86	-66317.94	-66379.24
a_1 [nT]	+66384.26	+66318.37	+66380.95
a_2 [nT]	+33196.44	+33159.64	+33189.73
a_3 [nT]	+16598.48	+16580.87	+16593.73
a_4 [nT]	+8298.79	+8291.02	+8299.54
a_5 [nT]	+4149.44	+4145.13	+4147.85
b_0 [counts]	+2052.80	+2056.80	+2050.20

Equations (3a) and (3c) transform the Experiment magnetometer's coordinate axes so that its Z-axis is parallel to the spacecraft's spin axis, while the magnetometer's X-axis lies in the spacecraft's X-Y plane. After this transformation, the Experiment magnetometer axes are approximately aligned to the coordinate axes of the spacecraft. They are not exactly aligned because the boom upon which this magnetometer sits is a flexible helical coil which can twist and bend due to thermal action, satellite motion, and initial deployment orientation. None of these factors are monitored. Consequently, the precise orientation of the Experiment magnetometer relative to the spacecraft's coordinates is unknown. Coarse estimates of this magnetometer's orientation can be made by comparing its vector magnetic measurements to those of the less accurate Navigation magnetometer, which is fixed in space relative to the spacecraft's coordinates.

The magnetic field values derived in eqs. (3a), (3b), and (3c) are referred to as the "Measured" vector components of the earth's magnetic field. However, the vector axes of the Experiment magnetometer are not precisely aligned perpendicular to each other. The "True" magnetic field vector components associated with an orthogonal set of axes are obtained from the "Measured" magnetic field components via the following alignment correction transformation:

$$\mathbf{B}_{True} = \mathcal{M}\,\mathbf{B}_{Measured} \qquad (4)$$

where the 3 x 3 transformation matrix, the elements of which are dimensionless, is:

$$\mathcal{M} = \begin{pmatrix} 1.0000 & -7.8196\times10^{-5} & -3.2410\times10^{-4} + \sum_{n=1}^{5}\gamma_{1n}B_z^n \\ -3.0890\times10^{-3} & 0.9999 & 1.2820\times10^{-2} + \sum_{n=1}^{5}\gamma_{2n}B_z^n \\ 8.6150\times10^{-3} + \sum_{n=1}^{5}\gamma_{3n}B_z^n & 2.9630\times10^{-4} & 1.0000 \end{pmatrix} \quad (5)$$

The cross coupling constants γ_{mn} are listed in Table 4. Further details concerning these DMSP-type magnetometer calibrations, with respect to the determination of magnetometer calibration coefficients, scale factors, and orthogonality factors, are discussed by Chomay (1987).

The third step in the calibration procedure is to correct for ambient temperature fluctuations. POGS has two temperature sensors, one to monitor the magnetometer's electronics package, denoted as T_E, and one to monitor the magnetic sensor, denoted as T_S. The former is onboard the spacecraft and the latter is at the tip of the boom and therefore will always measure slightly colder temperatures. The temperature correction factors are referenced to room temperature (20° C). Each axis of the magnetometer has its own correction factor. The temperature corrections applied to $B_{T_{true}}$ using the sensor temperature T_S are:

$$B_x = [1.0 + 0.000080(T_S - 20)]B_{x(T_{true})} \quad (6a)$$

$$B_y = [1.0 + 0.000046(T_S - 20)]B_{y(T_{true})} \quad (6b)$$

$$B_z = [1.0 + 0.000047(T_S - 20)]B_{z(T_{true})} + 7.0 \quad (6c)$$

Table 4. POGS Experiment Magnetometer Cross Coupling Constants γ_{mn}

n	γ_{1n}	γ_{2n}	γ_{3n}
1	-3.670×10^{-9}	-1.122×10^{-8}	$+4.527 \times 10^{-9}$
2	-6.586×10^{-13}	-3.949×10^{-13}	-7.066×10^{-13}
3	$+2.526 \times 10^{-18}$	$+7.617 \times 10^{-18}$	-3.747×10^{-18}
4	$+3.070 \times 10^{-23}$	-1.303×10^{-23}	$+6.059 \times 10^{-23}$
5	-4.633×10^{-28}	-1.317×10^{-28}	$+7.877 \times 10^{-28}$

The last correction to the Experiment magnetometer observations accounts for the magnetic field generated by the body of the spacecraft and sensed at the tip of the magnetometer boom. Laboratory measurements found that the only correction required was the addition of a 7 nanoTesla bias to the Z-component of the temperature-corrected field. This bias has been included as part of the Z-component temperature correction of eq. (6c). This bias does not include corrections for the radiative effects of the two navigation tracking beacons which are turned on for about 20 seconds of each minute. The magnetic field sensed at the tip of the boom due to these beacons is on the order of 3 or 4 nanoTeslas. However, no corrections for the magnetic effect of the beacon transmissions were applied to the data. Instead, a flag is set when the beacons are on. Then, for modeling purposes only unflagged data are selected.

3.0 SUN SENSOR ATTITUDE

The POGS satellite has 52 solar panels. Some of these panels have been configured as sun sensors in order to roughly determine the satellites attitude relative to the Sun-line. The parameters measured are the Azimuth and Elevation of the spacecraft relative to the Sun-line. The accuracy of these parameters is not known, but they are certainly no more accurate than $\pm 3^{\circ}$ under the best of circumstances. The accuracy degrades as the earth's dawn-dusk meridian is approached from the sun-side. The + Z axis of the sun sensor coordinate system is parallel to the spacecraft's spin axis, which, because the satellite was inserted into orbit upside-down, is Earth-Pointing. However, the X-axis and the Y-axis of the sun sensor coordinate system are rotated 11.25° counterclockwise with respect to the corresponding spacecraft axes as indicated in Figure 3. In this figure, the satellite's +Z axis, which is Earth-Pointing, is directed out of the page. Simply used as sun sensors, the solar panel data are valuable in determining when the

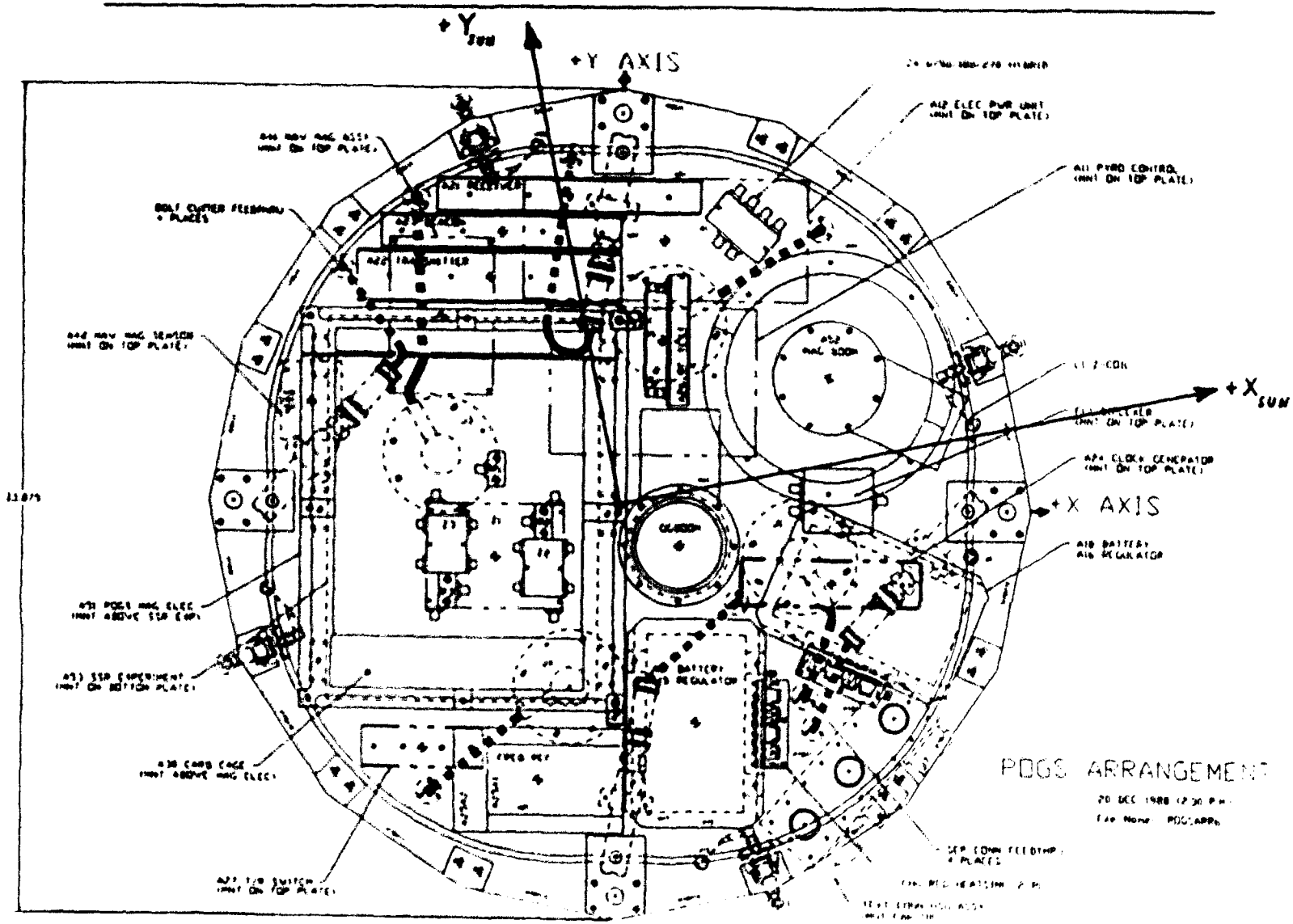

Figure 3. Interior Schematic of POGS Satellite: Sun Sensor X-Y Axes are Rotated 11.25° Counterclockwise with Respect to Spacecraft X-Y Axes

satellite is on the sun-side of the earth and when it is in the earth's shadow. This permits easy interpretation of the magnetic field responses along each orbit as being of crustal origin or of external ionospheric or magnetospheric origin.

4. SATELLITE POSITIONING

There are two tracking beacons on the POGS satellite. Each beacon has its own transmitter frequency. The beacons are tracked by the TRANET global network of tracking stations, the data from which are supplied to DMA, which in turn processes the tracking data using sophisticated orbit determination programs developed by the Naval Surface Weapons Center's Dahlgren Laboratory in Dahlgren, VA. The POGS satellite tracking data processed by DMA are referenced to the GEM-10B gravity model. Numerous tidal, ionospheric, and atmospheric corrections are applied to the tracking data. The final ephemeris (i.e., orbit determination) is supplied to NAVOCEANO at 1-minute time intervals in Earth-Centered, Earth-Fixed coordinates, relative to the coordinate system of the GEM-10B ellipsoid, with a spherical probable error (SEP) of less than 75 meters. Further details concerning satellite orbit determination are discussed by James W. O'Toole (1976) and by Cappellari et al. (1976). Relevant information concerning geodetic positioning is given by Mueller and Eichhorn (1977), while relevant information concerning earth rotation is given by Moritz and Mueller (1987).

Due to the recent completion of the Global Positioning System (GPS) network of satellites, DMA has made the decision to dismantle its ground-based global satellite-tracking network and its data processing support group beginning in October 1993. Consequently, the status of the POGS satellite, which is still expected to be operational at that time, then comes into question.

There are alternative sources for this tracking data. The possibility of acquiring ephemeris data from these alternative sources is now being investigated.

5. POGS CLOCK CALIBRATIONS AND DATA TIME SYNCING

The quartz-crystal clock on the POGS satellite is accurate to about one part in 10^7 and has a substantial linear drift which is occasionally interrupted by discontinuous jumps. The drift and discontinuous jumps in the POGS clock readout can accumulate to a timing error of several seconds over the course of several months. Consequently, it is necessary to periodically calibrate the POGS clock.

The POGS quartz-clock calibration procedure involves the transmission of a 20-second timing-pulse from the spacecraft to the Master ground station located at NAVOCEANO, Stennis Space Center, MS. The start-time and end-time of each pulse are known a priori from pre-determined schedules telemetered to the satellite. Due to the fact that the onboard computer may be performing other tasks when a particular timing-pulse is intended to begin, the timing-pulse may not begin exactly when scheduled. In this event, the timing-pulse is automatically shortened so that it ends exactly 20 seconds after its intended start-time. Thus, measuring the time that the trailing edge of the timing-pulse reaches the Master ground station using a cesium time standard, making corrections for the pulse travel-time from the satellite to the ground station, and subtracting the intended end-time of the timing-pulse, yield the time difference between the POGS clock and Naval Observatory (Universal) time to which the cesium standard is calibrated. The Master ground station's cesium standard clock is accurate to within a few microseconds per year and is therefore quite stable.

The travel-time correction computation requires knowledge of the slant-range $R_{(slant)}$ between the satellite and the ground station. The slant-range is determined from an orbit computation algorithm developed by DSI, the prime contractor responsible for building the POGS satellite and for writing the satellite and ground station software. The orbit parameters for this algorithm are regularly updated using values supplied by the Air Force's Satellite Tracking Facility at Cheyenne Mountain, CO. With the slant-range given in nautical miles, the travel-time correction in seconds is given by the following formula:

$$T_{(travel)} = 6.183 \times 10^{-6} R_{(slant)} \tag{7}$$

The time differences between the POGS clock and the cesium standard clock for the period from January 1991 to June 1993 are plotted in Figure 4. Their actual numerical values are listed in Table 5. Figure 4 indicates that the POGS clock generally runs a few seconds ahead of the cesium standard clock. Disjoint linear drift segments ranging in duration from a few days to more than a month in length are clearly evident. Occasionally, the computed time differences are significantly in error. These errors can be attributed to unusual ionospheric or atmospheric conditions which occurred during the timing pulse and also to human error. These errors produce the occasional but obvious anomalies seen in Figure 4 and are discarded before determining the POGS clock corrections.

The POGS time correction procedure involves the identification of the beginning and end times for each time sub-interval for which the clock drift is linear and the determination of the clock-drift rate for each of these sub-intervals. The time tags attached to magnetics data acquired during a particular time sub-interval are then appropriately adjusted to coincide with

POGS CLOCK TIMING CORRECTIONS

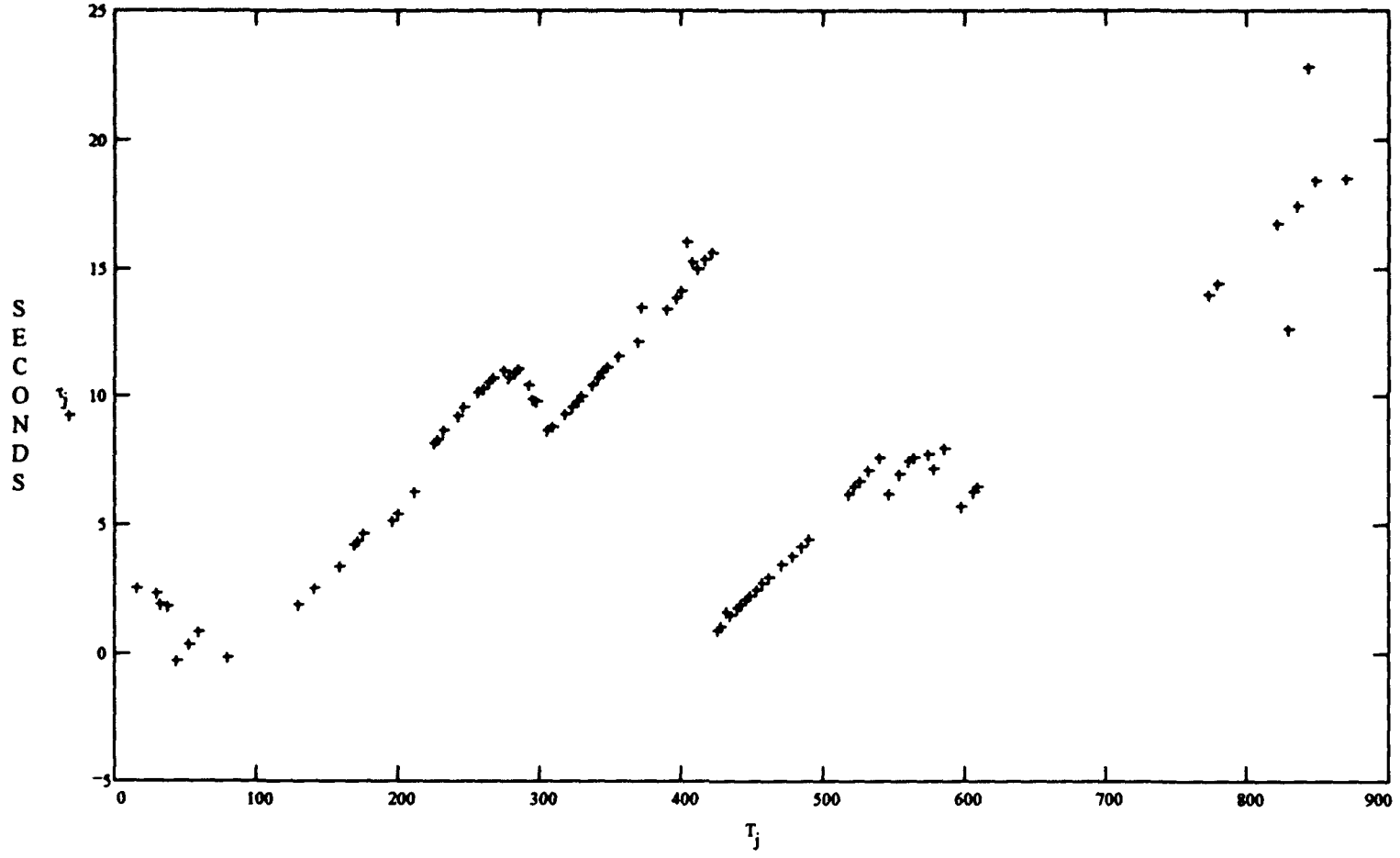

Figure 4. POGS Onboard Quartz-Clock Drift: POGS Time - Universal Time

Table 5. Timing Pulse Differences (POGS - UT); Units: Seconds

YEAR	DAY	DIFFERENCE	YEAR	DAY	DIFFERENCE
1991	015	+2.533	1991	241	+9.234
1991	030	+2.295	1991	246	+9.549
1991	032	+1.833	1991	256	+10.153
1991	037	+1.760	1991	259	+10.283
1991	043	-0.319	1991	263	+10.549
1991	052	+0.776	1991	266	+10.711
1991	079	-0.183	1991	273	+10.981
1991	129	+1.839	1991	277	+10.736
1991	140	+2.497	1991	281	+10.925
1991	158	+3.382	1991	284	+11.070
1991	169	+4.178	1991	294	+9.852
1991	171	+4.324	1991	297	+9.794
1991	175	+4.621	1991	304	+8.642
1991	196	+5.139	1991	308	+8.830
1991	200	+5.426	1991	308	+8.830
1991	211	+6.218	1991	322	+9.571
1991	225	+8.188	1991	326	+9.814
1991	227	+8.323	1991	329	+10.004
1991	232	+8.665	1991	336	+10.449

Table 5. Timing Pulse Differences (con.)

YEAR	DAY	DIFFERENCE	YEAR	DAY	DIFFERENCE
1991	340	+10.701	1992	073	+1.704
1991	343	+10.892	1992	076	+1.875
1991	347	+11.140	1992	080	+2.095
1991	354	+11.573	1992	083	+2.244
1992	003	+12.091	1992	087	+2.441
1992	006	+13.484	1992	092	+2.692
1992	023	+13.424	1992	097	+2.940
1992	030	+13.809	1992	106	+3.395
1992	034	+14.073	1992	113	+3.754
1992	038	+16.019	1992	120	+4.112
1992	041	+15.213	1992	125	+4.390
1992	045	+14.970	1992	153	+6.179
1992	050	+15.293	1992	157	+6.440
1992	055	+15.610	1992	160	+6.650
1992	057	RESET	1992	167	+7.114
1992	059	+0.853	1992	174	+7.620
1992	062	+1.040	1992	181	+6.173
1992	066	+1.602	1992	188	+6.985
1992	069	+1.469	1992	195	+7.470

Table 5. Timing Pulse Differences (con.)

YEAR	DAY	DIFFERENCE	YEAR	DAY	DIFFERENCE
1992	199	+7.567	1993	042	+13.945
1992	209	+7.768	1993	049	+14.381
1992	213	+7.615	1993	091	+16.740
1992	220	+7.913	1993	098	+12.586
1992	232	+5.688	1993	105	+17.446
1992	241	+6.279	1993	112	+22.776
1992	244	+6.472	1993	118	+18.427
1992	250	DOWN	1993	139	+18.484

Universal Time (UT). Identifying these time sub-intervals of linear POGS clock-drift requires careful analysis of the time difference data in Figure 4 and the comparison of that data with the magnetic total intensity data. The magnetic field data exhibit small anomalies when the POGS clock makes a discontinuous break from its linear drift trend. In this way the start-time and end-time of each linear clock-drift time sub-interval can be determined to within a few milliseconds. However, ionospheric and magnetospheric magnetic disturbances can occasionally interfere with and reduce the accuracy of this process.

In addition to the clock-drift corrections, there is one rather small time correction of 0.51 milliseconds applied to the data. This correction arises from a timing delay on the POGS clock-timer board. When all of the timing corrections are applied to the data, the overall timing error associated with the data is expected to be on the order of 10 to 20 milliseconds for most of the data. The timing errors of the ephemeris data are of the same magnitude. Both data sets, having been synced with Naval Observatory time to the same accuracy, are then said to be synced with each other and are then merged by time. Since the ephemeris data is sent to NAVOCEANO at 1-minute time intervals, it must be interpolated in order to attach a position to each 10-second magnetic field measurement. Cubic spline interpolation is used on the Earth-Centered, Earth-Fixed rectangular coordinates of the DMA-supplied ephemeris.

6. DATA EDITING

The observed magnetic field data are not completely clean. During the course of a single orbit, the satellite encounters numerous radiation hits, some of which may alter computer chip memory bits through some ionization process. The altered data appear as a set of spikes in the total intensity as indicated in Figure 5. These spikes are flagged using an interactive

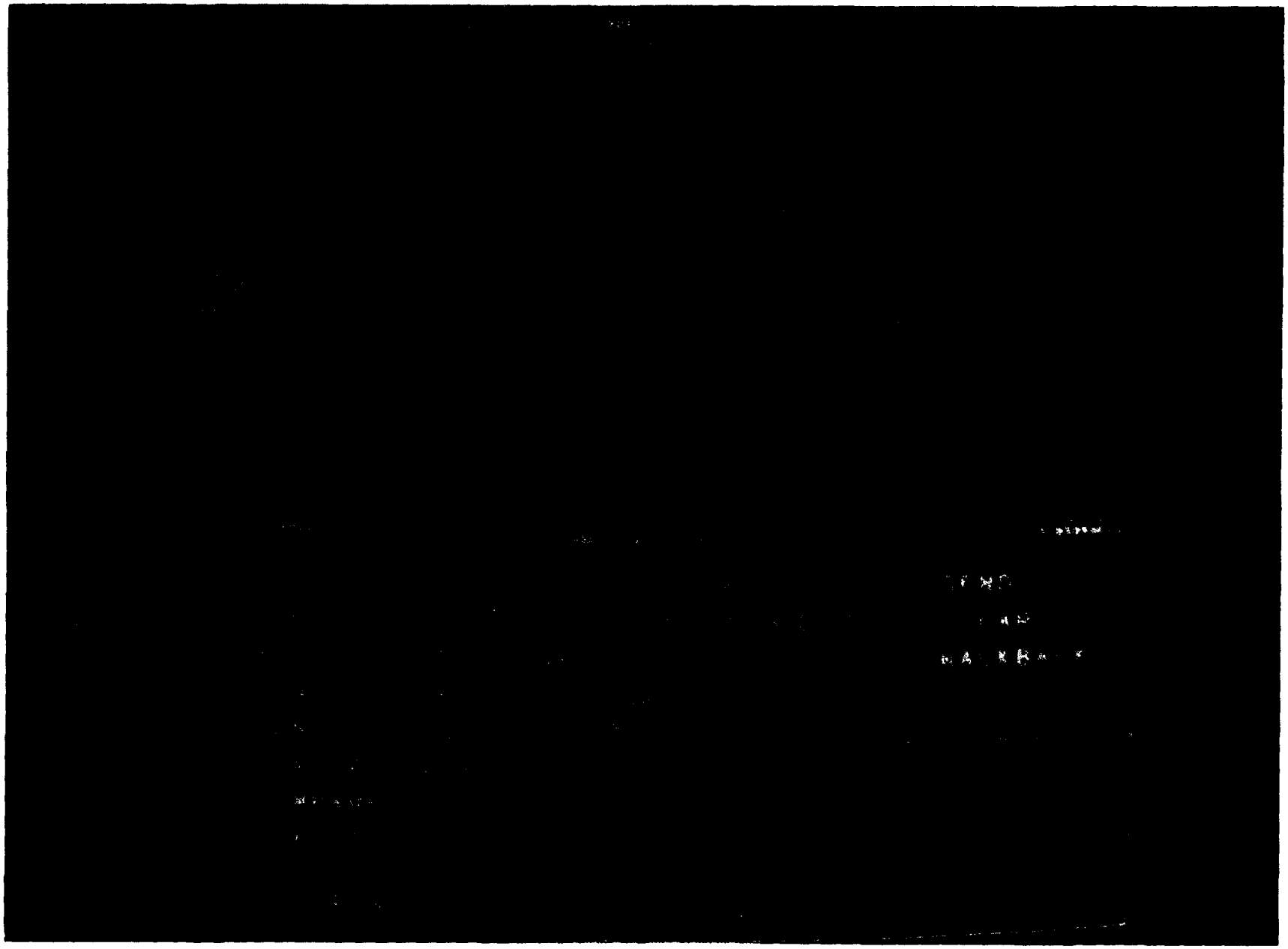

Figure 5. POGS Uncalibrated/Unedited Total Intensity Residual Profile Computed with Respect to the WMM-90 Model: Covers 13379.1 Seconds (2 Orbits); the Large Oscillations are the Phase Differences Between POGS Data Uncorrected for Clock Drift and the WMM-90 Model; the Spikes are Due to Radiation Encountered in Space; the Interval Between Small Tick Marks on the Vertical Axis Corresponds to 100 nT

graphics editor. An edit flag set to "0" for good data and set to "1" for bad data is attached to each observation. A similar flag is used to indicate when the tracking beacons are turned on and off. A data record is considered to be a valid magnetic field measurement when both flags are zero.

7. PRELIMINARY MODELING OF POGS DATA

The POGS satellite orbit is a polar one and has an average altitude of approximately 688 km. The most significant ionospheric current systems are in the altitude range of 100 km to 200 km. These current systems include the auroral electrojets in the north and south polar regions and the equatorial electrojet which straddles the geomagnetic equator. Although the currents in these regions are generally well defined and localized except for periods of magnetic storms, the fields that they generate frequently affect the ambient magnetic field at mid-latitudes. Additionally, there are a variety of magnetospheric currents located several earth radii above the POGS satellite orbit that also generate fields that can be sensed by the POGS satellite's Experiment magnetometer. The most significant magnetospheric source of magnetic fields is the Ring current, which surrounds the earth in the equatorial plane. Finally, there are field-aligned current systems which couple the magnetosphere to the ionosphere in the polar regions. Since POGS is a polar orbiting satellite, it will pass directly through the field-aligned currents, and during certain periods of heightened solar activity, its magnetometer may measure magnetic fields generated by these field-aligned currents on the order of a thousand nanoTeslas or more.

It is our intended purpose to globally model only the main (core-generated) magnetic field of the earth using POGS data. This means that the remnant and induced magnetic fields generated

by the earth's crust, as well as those magnetic fields generated by exoatmospheric electric currents that exist between the ionosphere and the magnetosphere, must be separated from those generated within the earth's core. This separation is accomplished in several different ways. The height of the satellite above the earth's surface is an effective filter of the crustal fields. To assist in the effort of separating the exoatmospheric fields, the National Geophysical Data Center (NGDC) in Boulder, CO, computes the planetary K (K_p) index which monitors the magnetic effect of solar activity at 3-hour intervals. This index ranges in value from 1 to 10, with 1 corresponding to solar quiet periods and 10 corresponding to solar disturbed periods.

Our first task is to select POGS data on the basis of the K_p index. Generally, data with an index equal to or less than 2^+, which corresponds to the most magnetically quiet times, are selected for modeling. Then, from this magnetically quiet set of data, we select data on the basis of local time. The magnetically quietest part of the day is between 9 p.m. and 6 a.m. We also select data on the basis of season. Generally, the magnetically quietest part of the year is during the three winter months for the north and south hemispheres. Additionally, a priori global magnetic field models do exist which can be used as references. The residual fields from these a priori models can be used to visually edit and remove from the data, via interactive computer graphic techniques, the effect of the exoatmospheric currents on the satellite measurements. External fields due to magnetospheric and ionospheric effects can also be modeled out in a phenomenological manner using the Disturbance Storm Time (Dst) index, which is another measure of magnetic activity, usually attributed to Ring current effects, but more recently also attributed in large part to field-aligned current effects. An example of the Dst index generated by M. Sugiura for the Magsat mission (1979 to 1980) is illustrated in Figure 6. For solar quiet times in the dawn-dusk orbit of Magsat, this index was typically less than 50 nT and had a

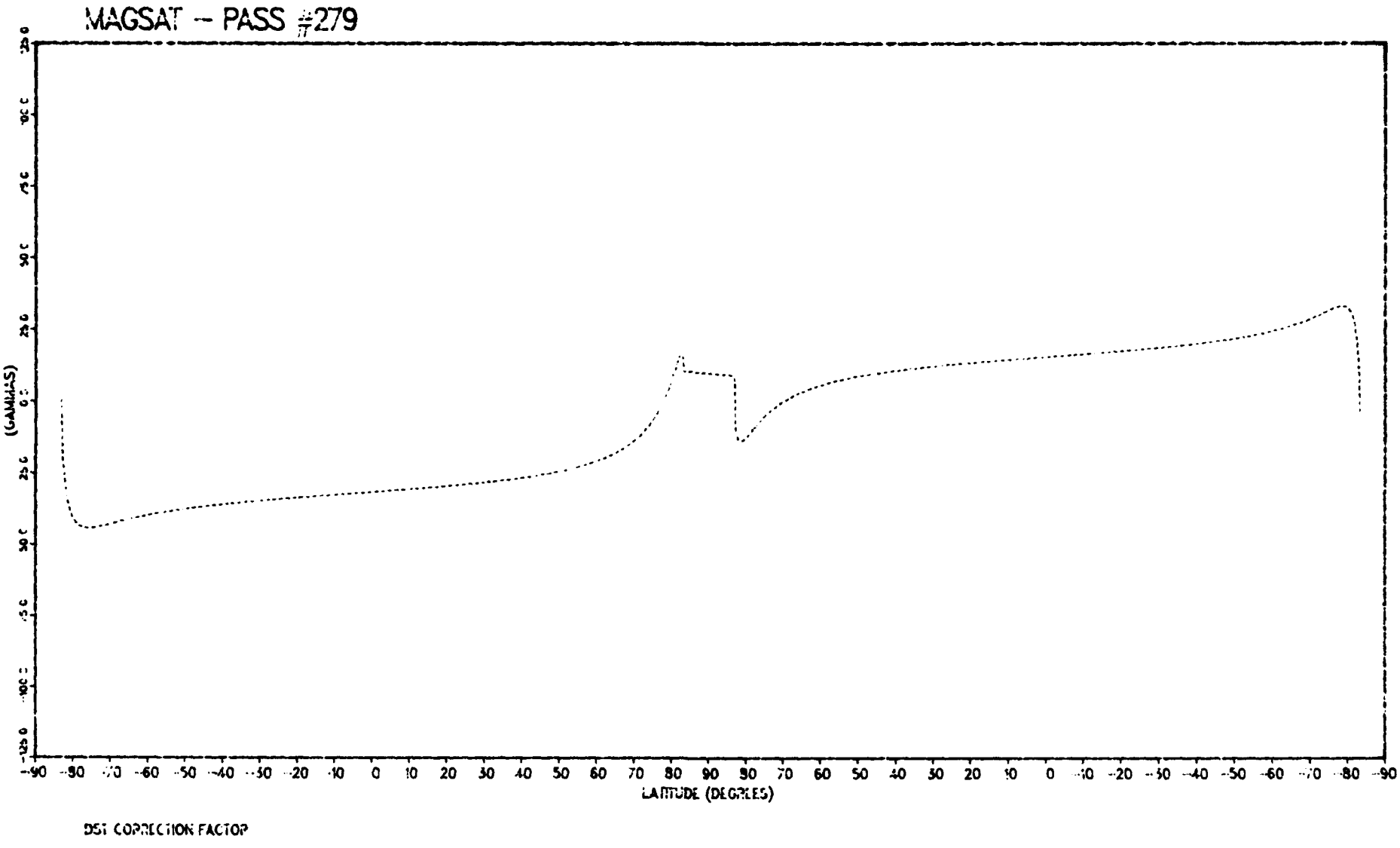

Figure 6. The Dst Index During One Magsat Orbit (Units: nT)

distinctive latitudinal variation as shown. A revised and improved method of generating the Dst index, which we call the Modified Dst index, is being generated for the POGS data by Wallace Campbell (*in Press)* of the U.S. Geological Survey in conjunction with NGDC. During quiet times, the magnitude of this index for POGS data will be substantially greater than 50 nT since POGS will see all local time, not just dawn and dusk as with Magsat. To minimize this source of noise, we restrict our data selection to the night side of the earth.

Finally, we can, as part of the core-field spherical-harmonic modeling process, include terms in the model, which correspond to external field effects and thereby model out the longer wavelength magnetospheric contributions to the measured field. The only exoatmospheric magnetic fields for which we cannot account for, even in a phenomenological manner, are the mid-latitude ionospheric current system effects even though much is known about them (Campbell [1989]). Generally, these are weak current systems, particularly during magnetically quiet times for which the K_p index is 2^+ or less, and for the most part are ignored.

The model presented in this report is preliminary in nature. This means that the POGS data selected for this model, though edited for radiation-induced spikes and POGS beacon transmissions, were not edited for exoatmospheric current effects. The data were selected for a K_p index of 2 or less. The data were also selected to reside within local times between 9 p.m. and 3 a.m. in order to minimize the effect of magnetic fields generated by solar heating/ionization of the upper atmosphere and ionosphere. The data selected covered the months of January and February 1991. Consequently, the winter season was in progress in the northern hemisphere, while the summer season was in progress in the southern hemisphere. No seasonal corrections were performed. Furthermore, no corrections for Dst were performed since the Dst indices were not yet available.

7.1 The POGS Preliminary Model

A spherical-harmonic model through internal degree 12 and external degree 2 was generated using 40,491 total intensity POGS data values, with a mean Epoch τ corresponding to day 34 of 1991. The potential field model is of the following mathematical form:

$$V(r,\theta,\varphi,\tau) = a\sum_{n=1}^{12}\sum_{m=0}^{n}\left(\frac{a}{r}\right)^{n+1}\left[g_{nm}(\tau)\cos m\varphi + h_{nm}(\tau)\sin m\varphi\right]P_n^m(\theta) + a\sum_{n=1}^{2}\sum_{m=0}^{n}\left(\frac{r}{a}\right)^{n}\left[q_{nm}(\tau)\cos m\varphi + s_{nm}(\tau)\sin m\varphi\right]P_n^m(\theta) \quad (8)$$

where the parameter "a" is the mean radius of the earth (6371.2 km), the parameters g_{nm} and h_{nm} are the internal Gauss coefficients, and the parameters q_{nm} and s_{nm} are the external Gauss coefficients. The modeling objective was to determine these Gauss coefficients at the mean epoch τ of the data set. Subsequently, the internal Gauss coefficients were temporally adjusted to the 1990.0 Epoch using the Secular Variation portion of the 1990.0 Epoch International Geomagnetic Reference Field (IGRF-90) (IAGA WG V-8 [1992]) in order to compare the POGS preliminary model directly to other models of that epoch.

The magnetic field **B** is the negative gradient of this potential field V. That is:

$$\mathbf{B}(r,\theta,\varphi,\tau) = -\nabla V(r,\theta,\varphi,\tau) \quad (9)$$

The internal Gauss coefficients are assumed to be linearly dependent on time and are considered valid for time intervals on the order of 5 years or less. These coefficients are generally referenced to a base epoch of time T_{Epoch}, which in units of years is divisible by 5.

Thus, they take the following mathematical forms:

$$g_{nm}(\tau) = g_{nm}(T_{Epoch}) + \dot{g}_{nm}(\tau - T_{Epoch}) \tag{10a}$$

$$h_{nm}(\tau) = h_{nm}(T_{Epoch}) + \dot{h}_{nm}(\tau - T_{Epoch}) \tag{10b}$$

The coefficients g_{nm} and h_{nm} have units of nanoTeslas as do the coefficients q_{nm} and s_{nm}, while $\dot{g}_{nm}$ and $\dot{h}_{nm}$ are the secular rates of change of their corresponding internal Gauss coefficients.

The external Gauss coefficients are assumed to depend on the time-dependent Disturbance Storm Time index $Dst(\tau)$, when it becomes available, as follows:

$$q_{nm}(\tau) = \alpha_{nm} + \beta_{nm} D_{st}(\tau) \tag{11a}$$

$$s_{nm}(\tau) = \gamma_{nm} + \delta_{nm} D_{st}(\tau) \tag{11b}$$

In order to avoid generating spurious anomalies into the model via the Backus effect (Stern et al. [1980]), vector data from the IGRF-90 model were foliated at 1° intervals throughout a region straddling $\pm 20^{\circ}$ about the geomagnetic equator. The data were unweighted. The resulting model coefficients are given in Table 6, where they are compared with the 1990.0 Epoch U.S/UK World Magnetic Model (WMM-90) coefficients, which were based on 1979/1980 vintage Magsat data and on a Project MAGNET data set which spanned the decade of the 1980's and which has a mean age of 5 years with respect to the 1990 modeling epoch (Quinn et al. [1991]). The POGS model coefficients listed in Table 6 were temporally adjusted to the 1990 epoch from the mean modeling epoch of the POGS data, using the IGRF-90 secular

Table 6. Preliminary POGS Spherical Harmonic Model Gauss Coefficients (Internal) Compared to WMM-90 at 1990.0; Units: nT

		POGS		WMM-90	
n	m	g_{nm}	h_{nm}	g_{nm}	h_{nm}
1	0	-29800.8	0.0	-29780.5	0.0
1	1	-1852.8	5413.2	-1851.7	5407.2
2	0	-2113.5	0.0	-2134.3	0.0
2	1	3060.5	-2283.3	3062.2	-2278.3
2	2	1693.7	-386.6	1691.7	-384.3
3	0	1305.1	0.0	1312.9	0.0
3	1	-2241.5	-284.7	-2244.7	-284.9
3	2	1245.0	296.7	1246.8	291.7
3	3	807.4	-353.5	808.6	-352.4
4	0	937.4	0.0	933.5	0.0
4	1	783.9	247.4	784.9	249.4
4	2	325.1	-236.9	323.5	-232.7
4	3	-419.4	87.1	-421.7	91.3
4	4	138.7	-294.7	139.2	-296.5
5	0	-206.1	0.0	-208.3	0.0
5	1	356.7	39.3	352.2	40.8
5	2	245.3	154.0	256.5	148.7
5	3	-113.0	-151.5	-110.8	-154.6
5	4	-166.5	-66.8	-162.3	-67.6
5	5	-37.2	98.3	-37.2	97.4
6	0	58.7	0.0	59.0	0.0
6	1	60.9	-9.0	63.7	-14.7
6	2	61.9	79.8	60.0	82.2
6	3	-179.6	64.8	-181.3	70.0
6	4	3.3	-57.7	0.4	-56.2
6	5	17.5	-1.6	15.4	-1.4
6	6	-97.4	23.0	-96.0	24.6
7	0	75.9	0.0	76.1	0.0
7	1	-61.7	-76.2	-62.1	-78.6
7	2	2.5	-24.0	1.3	-26.7
7	3	27.9	2.9	30.2	0.1
7	4	0.8	22.2	4.7	19.9
7	5	4.8	18.8	7.9	17.9
7	6	10.2	-20.1	10.1	-21.5
7	7	2.0	-7.2	1.9	-6.8

Table 6. Preliminary POGS Model Comparison (Con.)

		POGS		WMM-90	
n	m	g_{nm}	h_{nm}	g_{nm}	h_{nm}
8	0	25.8	0.0	22.9	0.0
8	1	2.2	8.9	2.3	9.7
8	2	-3.5	-19.7	-1.2	-19.3
8	3	-9.0	6.9	-11.7	6.6
8	4	-12.9	-21.1	-17.5	-20.1
8	5	5.5	13.3	2.2	13.4
8	6	5.8	10.1	5.7	9.8
8	7	3.2	-19.3	3.0	-19.0
8	8	-6.6	-10.1	-7.0	-9.1
9	0	5.6	0.0	3.6	0.0
9	1	7.4	-19.4	9.5	-21.9
9	2	3.2	13.2	-0.9	14.3
9	3	-13.6	11.2	-10.7	9.5
9	4	7.8	-6.3	10.7	-6.7
9	5	-4.8	-7.4	-3.2	-6.4
9	6	-1.8	9.7	-1.4	9.1
9	7	7.1	7.7	6.3	8.9
9	8	0.3	-8.1	0.8	-8.0
9	9	-5.4	2.2	-5.5	2.1
10	0	-4.2	0.0	-3.3	0.0
10	1	-3.0	1.5	-2.6	2.6
10	2	2.0	0.6	4.5	1.2
10	3	-4.9	4.5	-5.6	2.6
10	4	0.7	4.1	-3.6	5.7
10	5	5.8	-4.6	3.9	-4.0
10	6	1.8	0.2	3.2	-0.4
10	7	1.2	-0.7	1.7	-1.7
10	8	2.4	3.2	3.0	3.8
10	9	3.0	-0.4	3.7	-0.8
10	10	0.7	-6.3	0.7	-6.5
11	0	2.6	0.0	1.3	0.0
11	1	-1.4	-0.6	-1.4	0.0
11	2	-1.3	0.3	-2.5	1.0
11	3	1.9	-1.1	3.2	-1.6
11	4	-0.5	-2.4	0.2	-2.2
11	5	-1.7	0.2	-1.1	1.1
11	6	-0.5	-0.8	0.3	-0.7
11	7	0.1	-2.4	-0.3	-1.7

Table 6. Preliminary POGS Model Comparison (Con.)

		POGS		WMM-90	
n	m	g_{nm}	h_{nm}	g_{nm}	h_{nm}
11	8	0.3	-1.8	0.9	-1.5
11	9	-1.0	-1.0	-1.1	-1.3
11	10	2.5	-1.2	2.4	-1.1
11	11	3.0	0.6	3.0	0.6
12	0	-1.8	0.0	-1.3	0.0
12	1	-1.7	2.4	0.1	0.7
12	2	0.8	1.2	0.5	0.7
12	3	1.0	1.5	0.7	1.3
12	4	1.1	-2.4	0.4	-1.5
12	5	0.0	0.1	-0.2	0.3
12	6	-1.5	0.8	-1.1	0.2
12	7	0.7	-0.3	0.9	-1.1
12	8	-0.6	0.9	-0.6	1.2
12	9	0.2	0.1	0.8	-0.2
12	10	0.3	-0.9	0.2	-1.3
12	11	0.5	0.6	0.4	0.6
12	12	0.2	0.6	0.2	0.6

variation model in order to make the comparison with the WMM-90 model coefficients. There are significant differences between some comparable lower order coefficients of the two models. This is partly due to the omission of ionospheric and magnetospheric corrections to the POGS data and partly due to errors in the WMM-90 model, *which is based on relatively old data.*

The purpose for generating this preliminary POGS model is to use it as a tool for further reduction of POGS data. In particular, the magnetic residuals from this model will resolve the field-aligned current effects very distinctly and thus permit the removal of these effects in subsequent models based on this data. Thus, the process of generating a global magnetic field model from POGS data is an iterative one. The model in Table 6 exhibited the following statistical properties with respect to the 40,491 POGS total intensity data values with $K_p = 2^+$ collected during the months of January and February 1991 that were used to generate the model:

Mean:	-10.99 nT
Standard Deviation:	22.91 nT
Root Mean Square:	25.41 nT

These statistics include the contributions of both the internal and external portions of the POGS preliminary model. The Gauss coefficients for the external field at the mean epoch of the POGS data subset are listed in Table 7. Since the preliminary field model ignored the effects of the field-aligned currents and the Dst index (i.e., $\beta_{nm} = 0$, and $\delta_{nm} = 0$ for all n and m), it is expected that subsequent, more detailed models will reduce these statistics substantially. Nevertheless, as they stand, the statistics are good.

Table 7. Preliminary POGS Spherical-Harmonic Model Gauss Coefficients (External) at Mean Epoch 1991 Day 34; Units: nT

POGS (external)			
n	m	q_{nm}	s_{nm}
1	0	9.9	0.0
1	1	-9.0	2.8
2	0	11.2	0.0
2	1	8.0	-4.8
2	2	0.0	-2.6

7.2 Analysis of POGS Residuals

The residual magnetic field is composed of magnetic fields generated by all sources except the earth's outer core. There is a tendency to expect the POGS residuals to be similar to Magsat residuals. In particular it is often commented that POGS data are rather noisy, with the implication that there may be something wrong with the calibration of the magnetometer or with the data reduction procedures. Though not explicitly stated, the implication is that the comparison is made with respect to the Magsat data set, with which there is great familiarity. There is actually nothing amiss with either the calibrations or the data reduction procedures. What some modelers seem to forget is that the Magsat mission was sun-synchronous, the satellite traversing in a dawn-dusk orbit. This is the least magnetically disturbed of all the possible orbits that one could choose. The POGS mission, on the other hand, is not sun-synchronous and therefore sees all local times. Most particularly, it sees the dayside local times between 6 a.m. and 6 p.m., which are more magnetically active due to day-side solar heating effects. Secondly, the altitude of the POGS satellite is roughly twice as high as that of Magsat. Consequently, the field-aligned currents through which POGS traverses are broader latitudinally than those through which Magsat traversed due to the divergence of the main magnetic field lines with altitude. This makes the job of removing the magnetic effects generated by field-aligned currents from the POGS data more difficult than for Magsat. The problem is further aggravated by the fact that only total intensity data is available from POGS, while Magsat had vector data. Figure 7 illustrates the anomalous magnetic field for three vector components observed by Magsat as it traversed through the field-aligned currents feeding the north and south pole auroral ovals. In contrast, a comparable POGS orbit is exhibited in Figure 8, where the top illustration exhibits total intensity data collected during a period of

Figure 7. Vector Magnetic Field Residuals During One Magsat Orbit Computed with Respect to the GSFC 12/83 Model: Clearly Illustrates the Field-Aligned Current Effect in the Polar Auroral Zones; the Vertical Axis Range is $\pm$ 1000 nT

moderate solar activity for which $K_p = 6$. The magnitude of the field-aligned current effect is much less than that of Figure 7 due to the divergence of the current at higher altitudes. For the same reason there is a distinct broadening of the inner and outer rings of the ovals in the two hemispheres and a general spreading of the oval toward the equator. The second graph on Figure 8 illustrates the temperatures of the magnetometer sensor electronics box (blue) and of the magnetometer sensor (yellow). The temperatures are characteristically stable, varying slowly within narrow limits. The third graph in Figure 8 exhibits the satellite attitude relative to the sun-line. There is no attitude information when the satellite is on the night-side of the earth.

Figure 9 exhibits data collected on orbit 6113 during a highly disturbed period for which $K_p = 8$. In this figure, it is possible to see a broadening of the auroral ovals in both hemispheres to mid-latitudes as well as the pronounced effect of the equatorial electrojet which has been enhanced dramatically by magnetic storm activity. The total intensity data in Figure 10 reflect moderate solar activity corresponding to $K_p = 4^+$ to 5^-. Notice that at the equator in the top graph there is a significant difference in the residuals between the day-side and the night-side of the earth as defined by the attitude data in the third graph in Figure 10. On the day-side, the equatorial electrojet contributes an additional 75 nT to 100 nT to the observed field. In contrast, Figure 11 depicts an unusually quiet magnetic field record collected from orbit 4106 for which the K_p index was between 1^+ and 2^-.

A low K_p index does not always indicate benign magnetic field effects from exoatmospheric sources. Figure 12 for orbit 4909 was collected during a period for which $K_p = 1$. At mid-latitudes, particularly in the southern hemisphere, there is a very pronounced anomaly which appears to be caused by some unexpectedly strong mid-latitude current system. The residual field displayed in Figure 12 is taken with respect to our preliminary POGS model. The

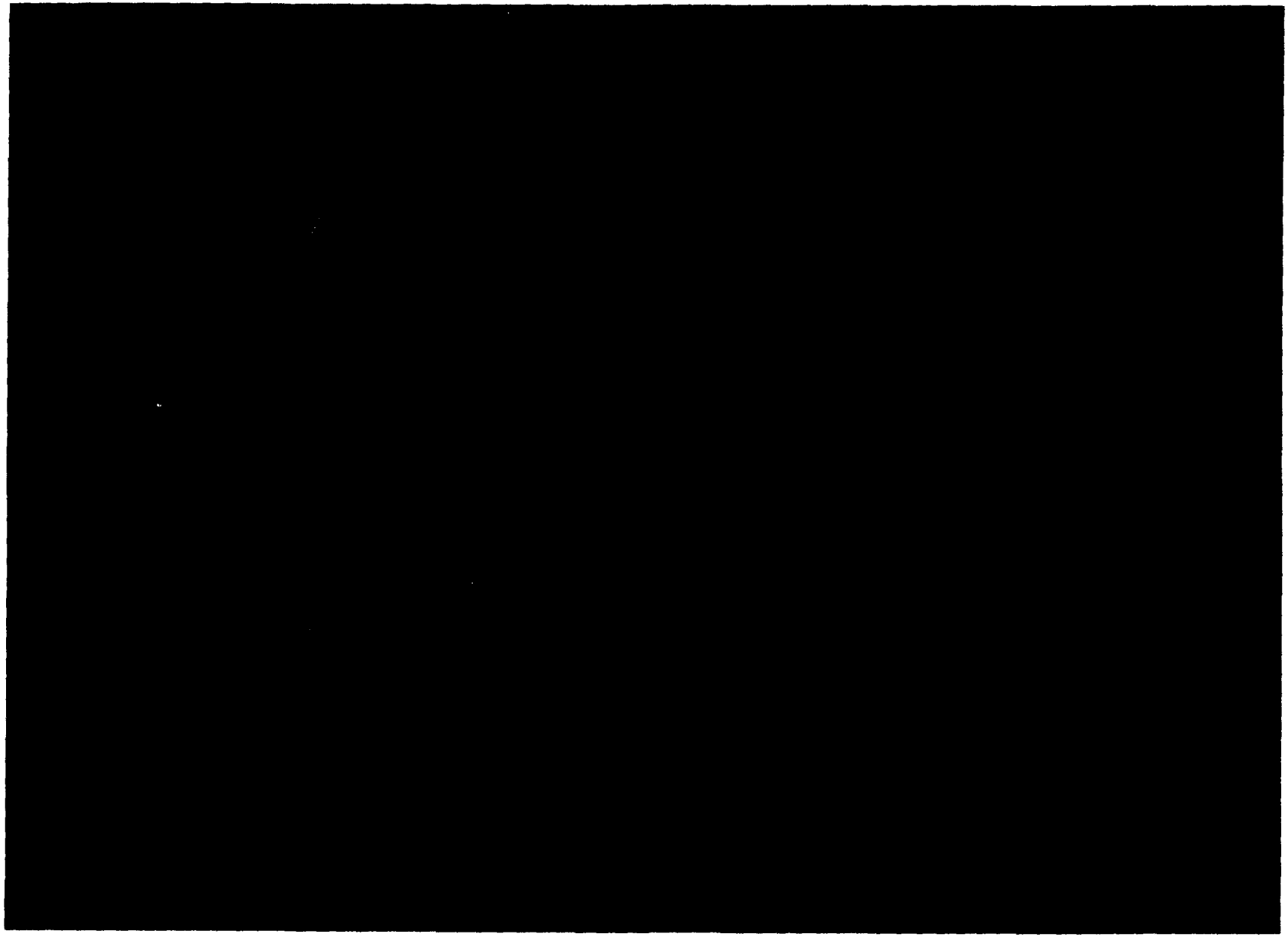

Figure 8. Total Intensity Residual Profile Computed with Respect to the Preliminary POGS Model and the Temperature and Attitude Profiles for Orbit #5825: $K_p = 6$

Figure 9. Total Intensity Residual Profile Computed with Respect to the Preliminary POGS Model and the Temperature and Attitude Profiles for Orbit #6113: $K_p = 8$

Figure 10. Total Intensity Residual Profile Computed with Respect to the Preliminary POGS Model and the Temperature and Attitude Profiles for Orbit #6679: $K_p = 4^+$ to 5^-

Figure 11. Total Intensity Residual Profile Computed with Respect to the Preliminary POGS Model and the Temperature and Attitude Profiles for Orbit #4106: $K_p = 1^+$ to 2^-

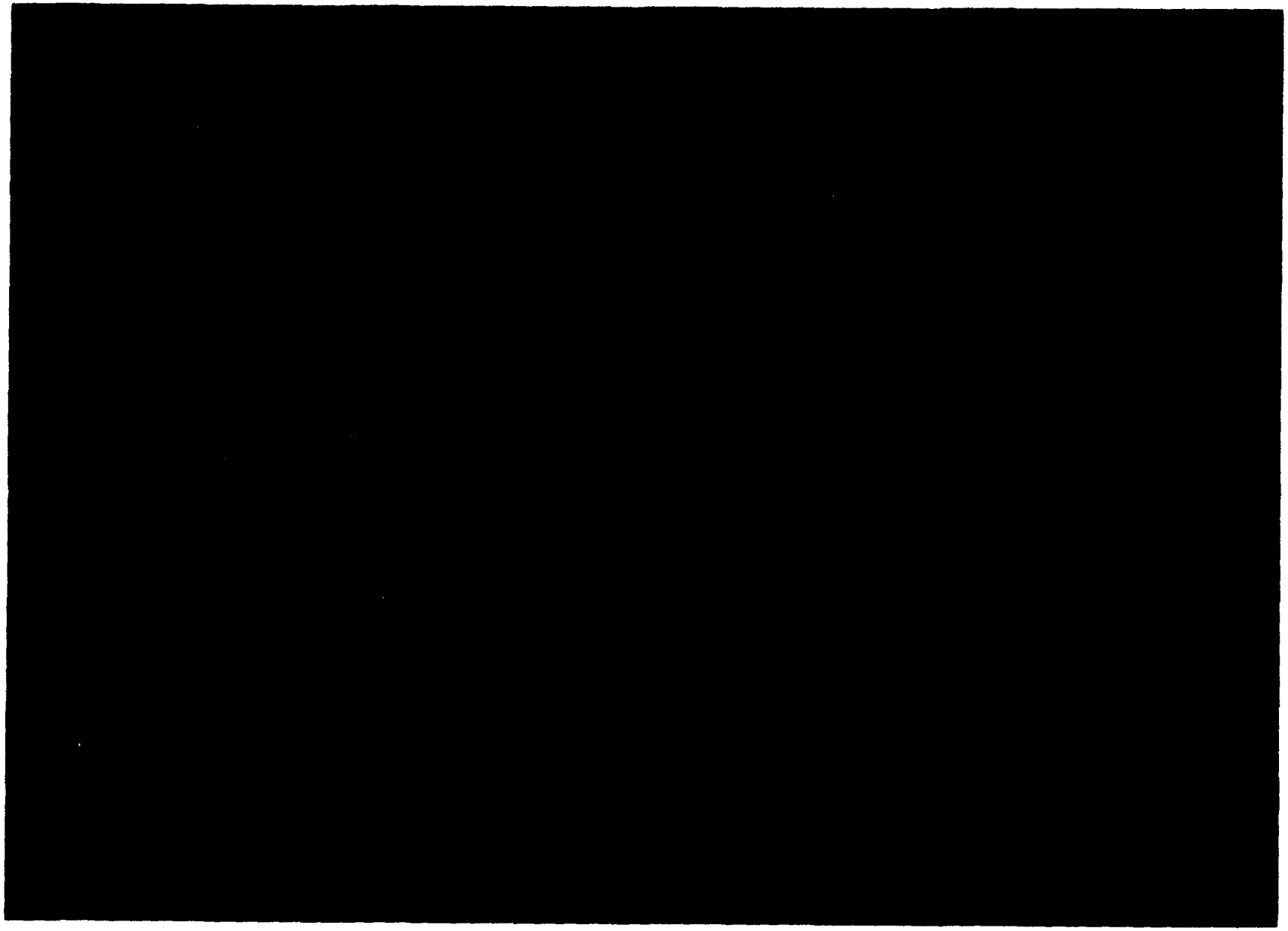

Figure 12. Total Intensity Residual Profile Computed with Respect to the Preliminary POGS Model and the Temperature and Attitude Profiles for Orbit #4909: $K_p = 1$

anomalous feature, however, is independent of the model used. The magnetic field total intensity residual generated from the IGRF-90 model for calendar day 73, 1991, exhibits the same feature. Therefore, this anomaly appears to be in the data and seems to be real, but is probably of external origin. Many of the POGS satellite profiles have this mid-latitude feature, though not always as pronounced as is illustrated in Figure 12. Furthermore, this feature persists in the southern hemisphere regardless of the season. There appears to be no comparable anomaly in the northern hemisphere regardless of the season. Until additional ionospheric and magnetospheric corrections are made to the data, our initial interpretation of this anomaly will remain tentative.

Finally, a direct comparison between residuals computed from the POGS preliminary model and the degree 10 IGRF-90 model are displayed in Figures 13 through 16. Figure 13 illustrates the POGS residual total intensity with respect to the POGS preliminary model for orbit 4044. Figure 14 is the IGRF-90 total intensity residual for the same orbit. For this orbit $K_p = 1$. The southern hemisphere mid-latitude anomaly is present to some extent in both figures. Note that on 1991 day 14 when these data were collected, it was mid-winter in the northern hemisphere and mid-summer in the southern hemisphere. As a second contrasting comparison, an orbit from 1991 day 173 was selected, which corresponds to early summer in the northern hemisphere early winter in the southern hemisphere. Figure 15 illustrates the total intensity residuals for the POGS preliminary model, while Figure 16 illustrates the IGRF-90 model total intensity residuals for the same orbit. The mid-latitude anomaly is not as evident in these figures. The K_p index for 6351 ranged between 3^+ and 4^-, corresponding to moderately active external geomagnetic activity as is indicated by the substantial auroral zone field-aligned current activity.

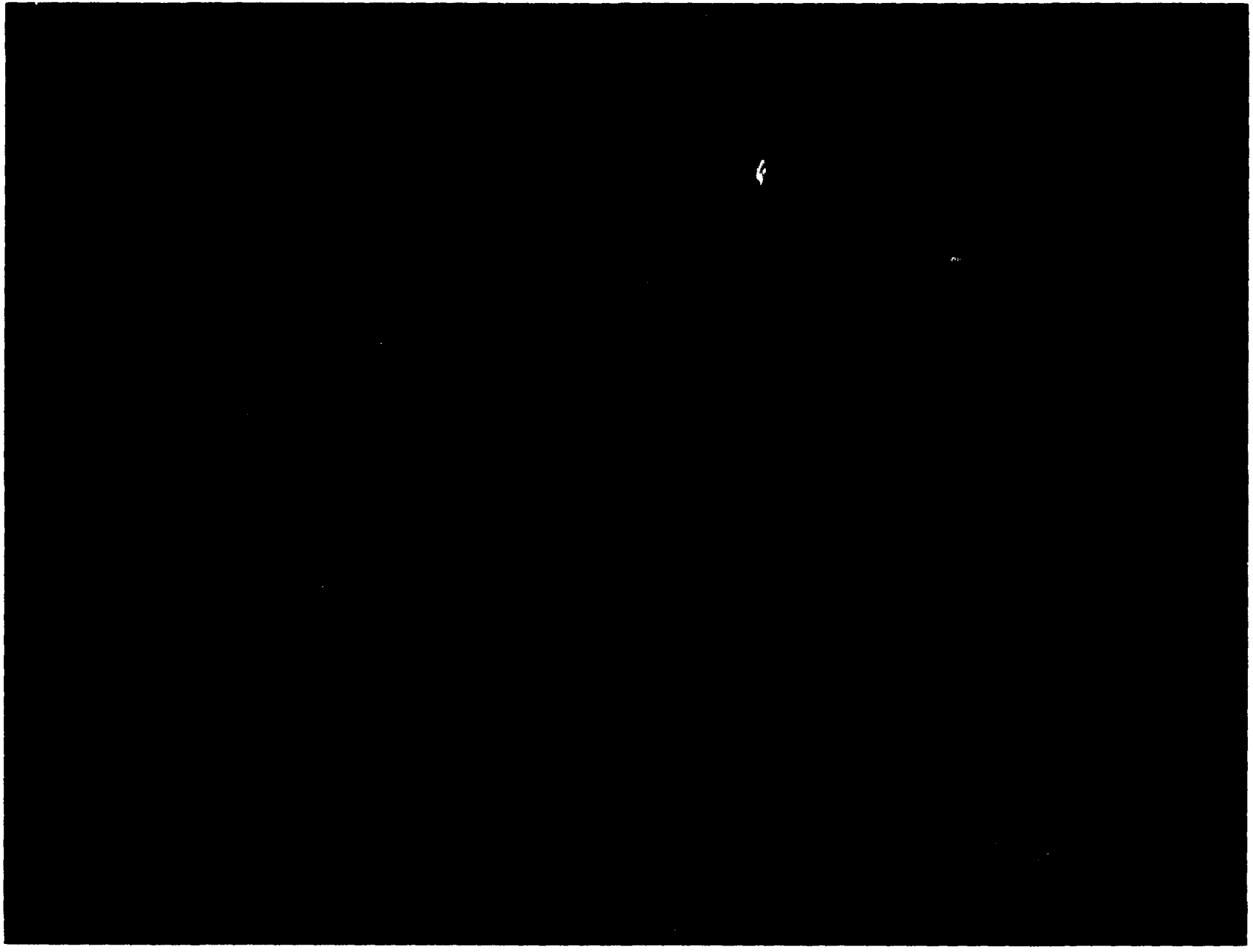

Figure 13. Total Intensity Residual Profile Computed with Respect to the Preliminary POGS Model and the Temperature and Attitude Profiles for Orbit #4044: $K_p = 1$

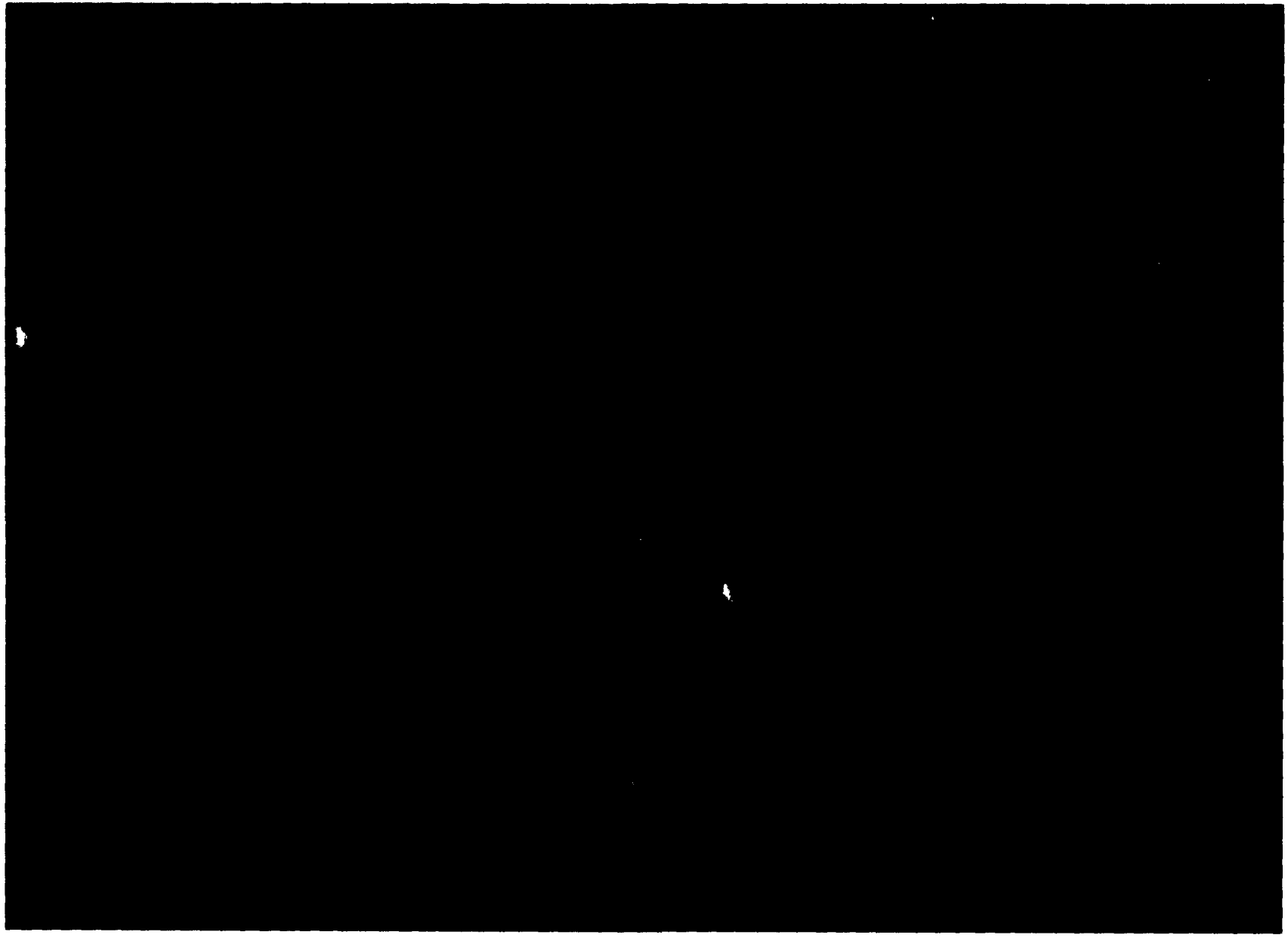

Figure 14. Total Intensity Residual Profile Computed with Respect to the IGRF-90 Model and the Temperature and Attitude Profiles for Orbit #4044: $K_p = 1$

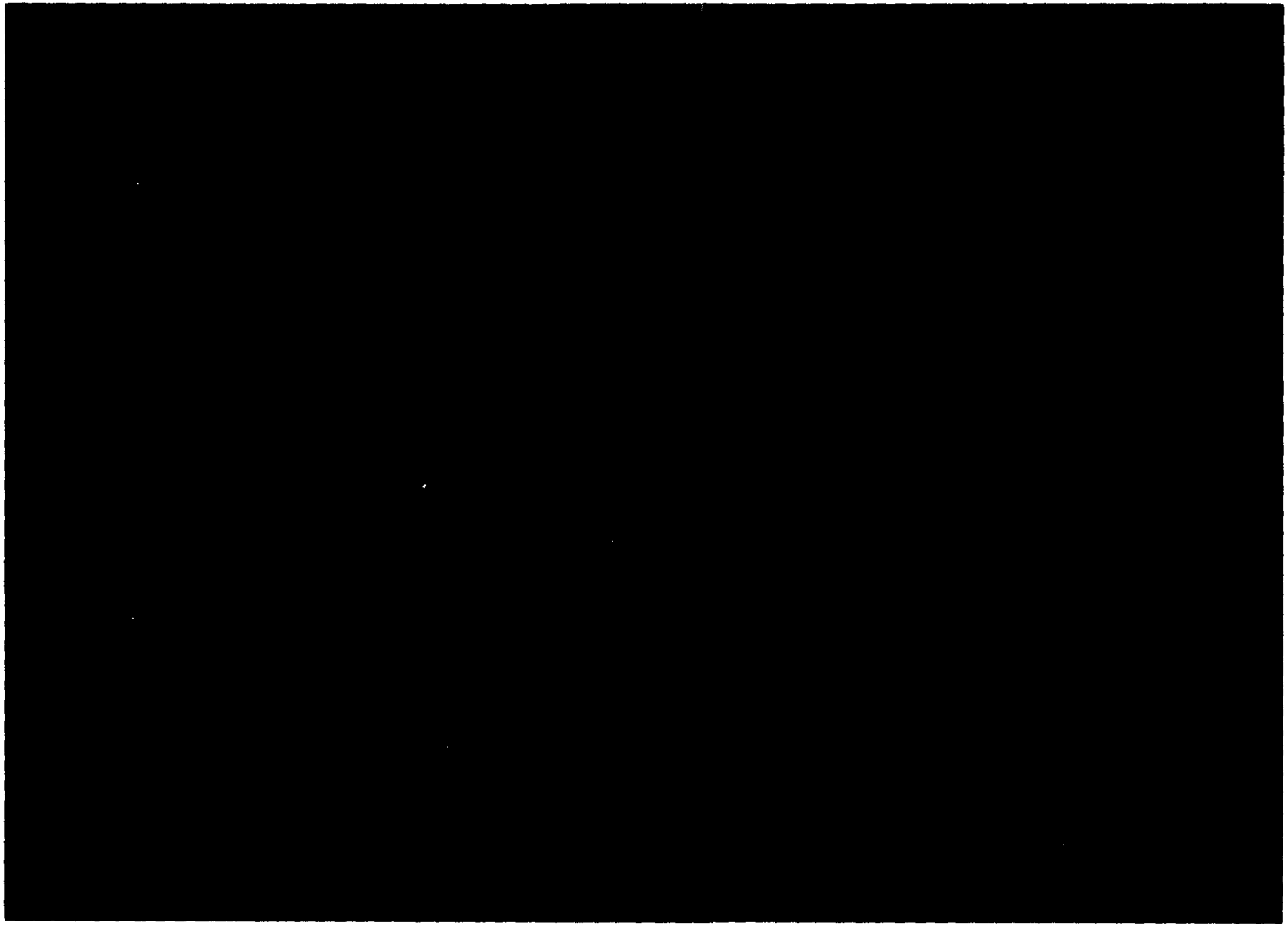

Figure 15. Total Intensity Residual Profile Computed with Respect to the Preliminary POGS Model and the Temperature and Attitude Profiles for Orbit #6351: $K_p = 3^+$ to 4^-

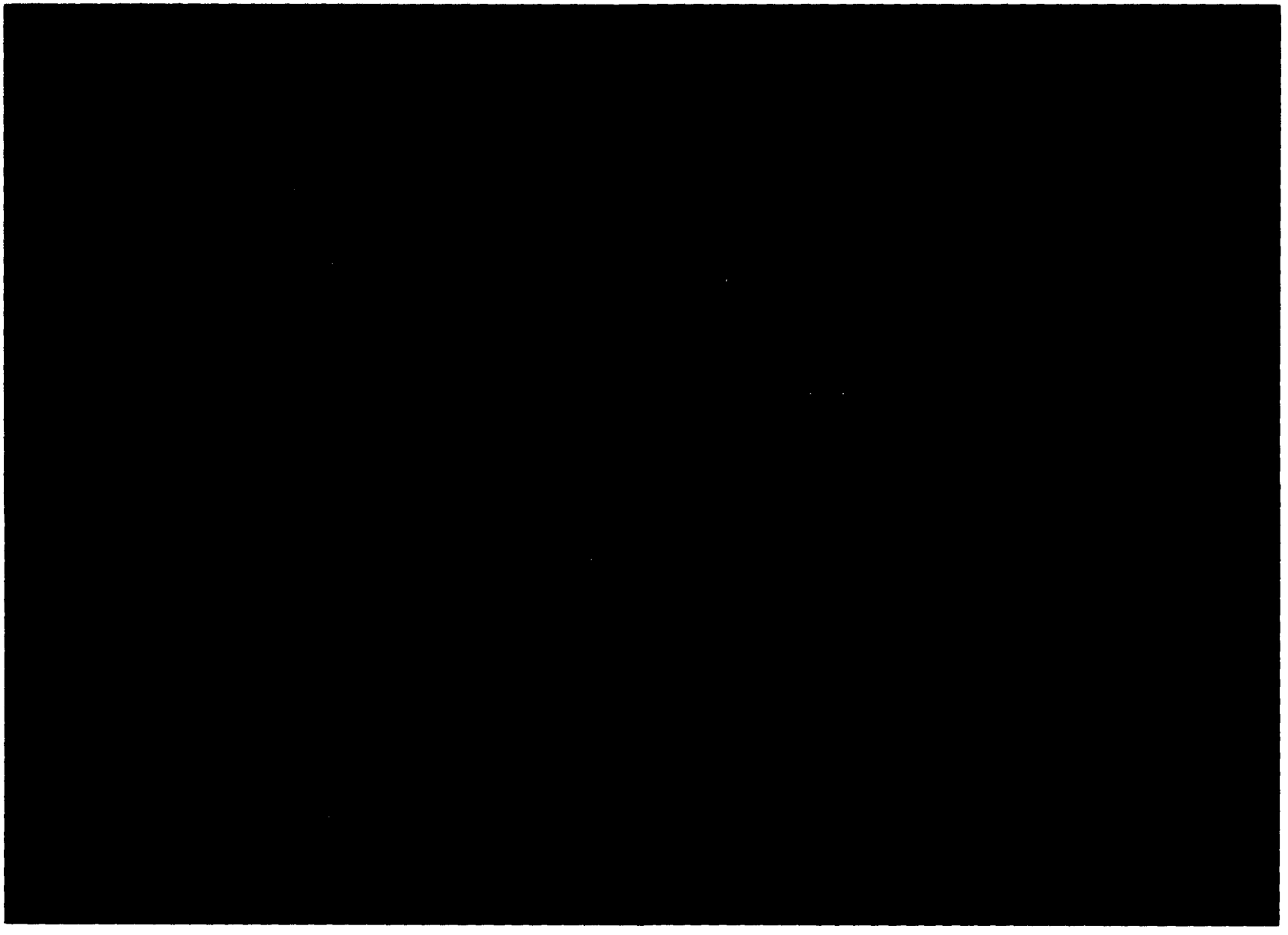

Figure 16. Total Intensity Residual Profile Computed with Respect to the IGRF-90 Model and the Temperature and Attitude Profiles for Orbit #6351: $K_p = 3^+$ to 4^-

8. FUTURE PLANS FOR THE 1995 EPOCH AND BEYOND

POGS data are intended to support the 1995 Epoch World Magnetic Model. In the coming months, these data will be meticulously edited for exoatmospheric current effects, and special Dst corrections will be applied. Rather than using data with K_p indices less that 2^+, as was the case with the preliminary model and other models based on Magsat data, only data with K_p indices less than 1^+ will be used. This is because of the large amount of POGS data that are available. Also, only data from the nightside and only data from the winter hemispheres will be used since seasonal effects do seem to be significant.

In the preliminary model presented in this report, the Backus effect was controlled by throwing in some vector data from a predictive model along the geomagnetic equator. In the 1995 Epoch model, real vector data collected from the Project MAGNET aircraft will be used. High-level Project MAGNET aeromagnetic surveys are currently being executed along the geomagnetic equator in the Atlantic, Pacific, and Indian oceans. Survey tracks that are either planned for the next 6 months or have already been collected in the Atlantic and Pacific oceans are illustrated in Figures 17 and 18. These data and some additional data collected in the Indian ocean will be sufficient to control the Backus effect.

Because of the longevity of the POGS satellite coverage and because of the spatial density of POGS survey coverage, the possibility arises that a sequence of models can be made to perhaps degree 20 or so, at 6-month intervals covering the period between 1991 through 1993. This sequence of main field models could be used to determine for the geomagnetic Secular Variation model for that time period to degree 12 or 15. This is in contrast to those of only degree 8 that are currently generated using data from a poorly distributed set of geomagnetic observatories.

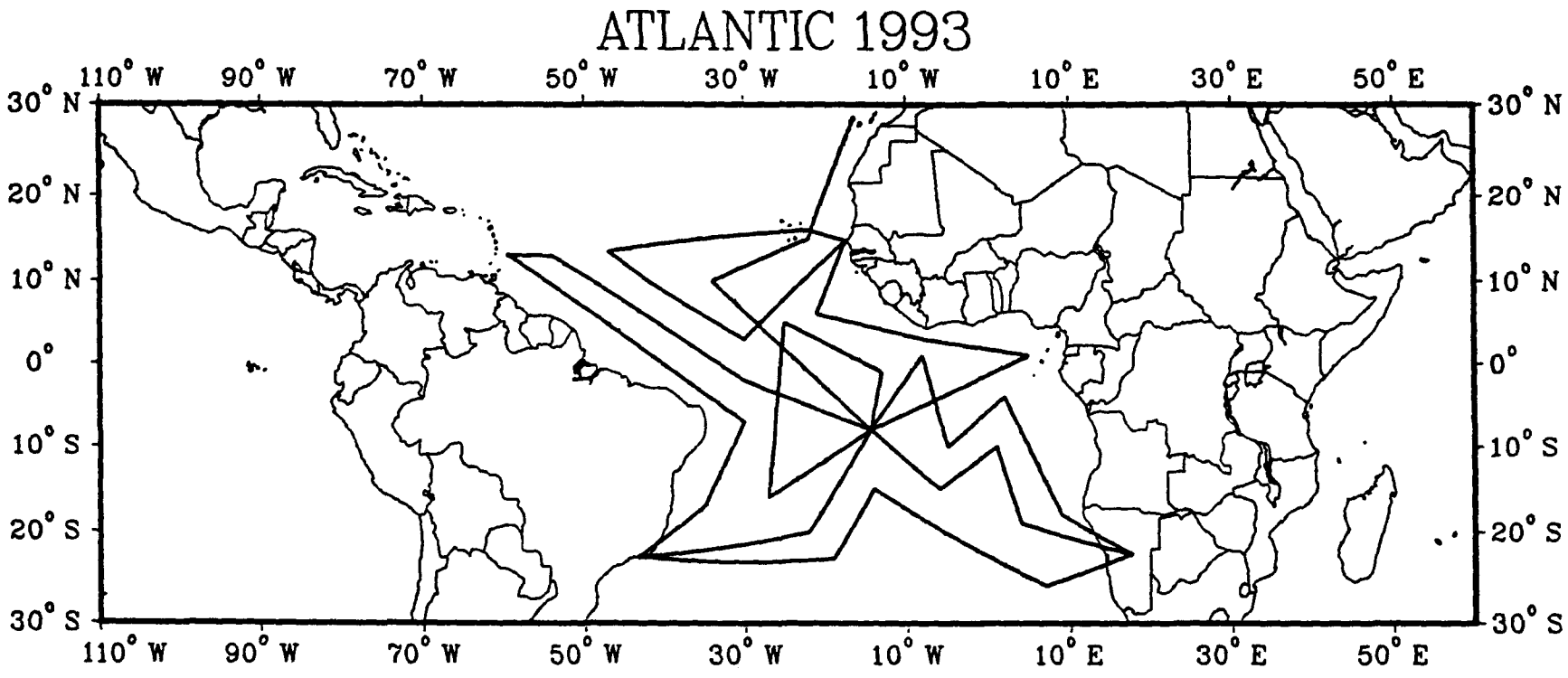

Figure 17. Project MAGNET Vector Magnetic Survey Plan (Atlantic): Intended to Counter the Backus Effect for the 1995 Epoch World Magnetic Model

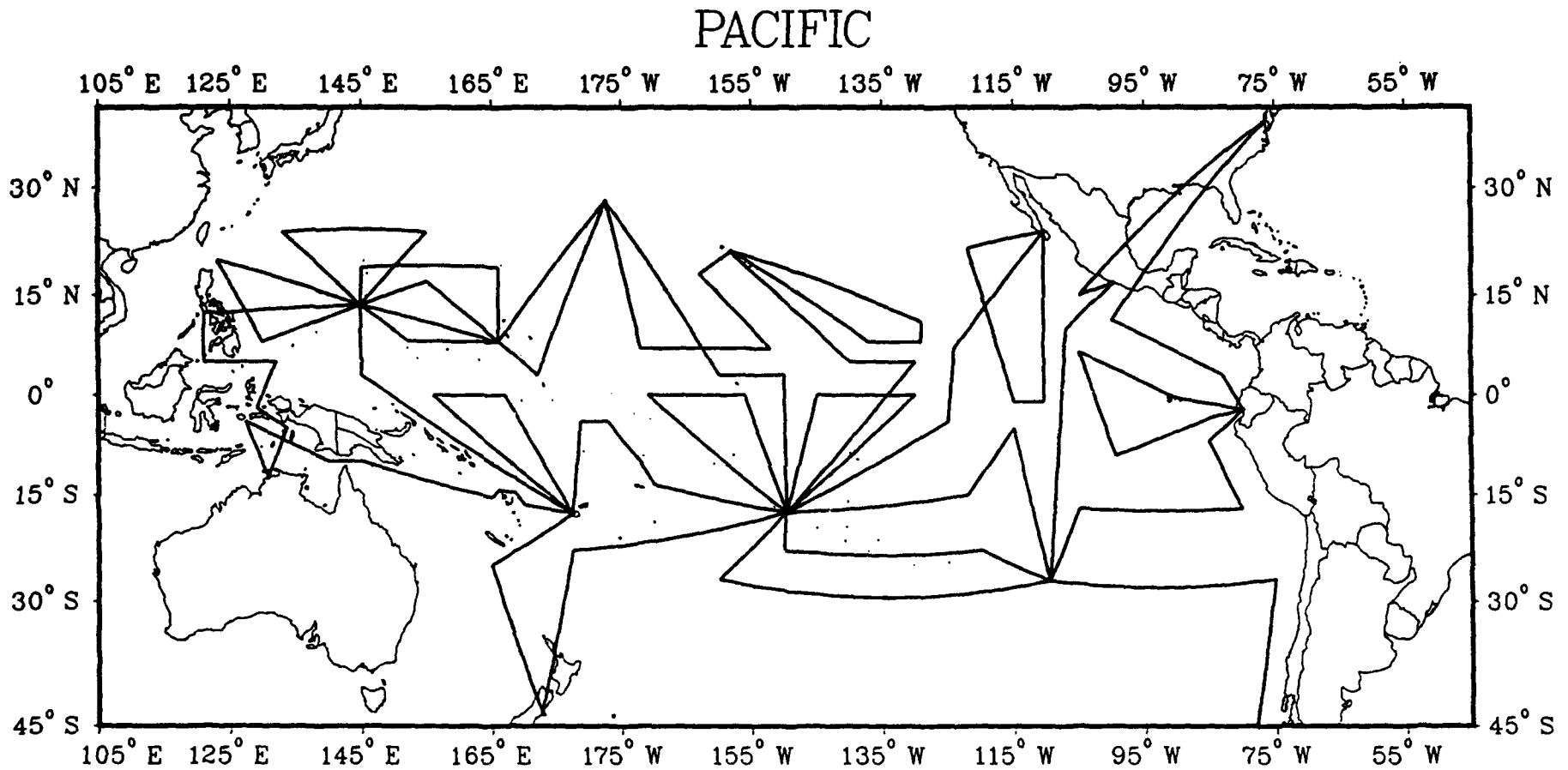

Figure 18. Project MAGNET Vector Magnetic Survey Plan (Pacific): Intended to Counter the Backus Effect for the 1995 Epoch World Magnetic Model

Finally, with respect to efforts to secure data for future modeling epochs, it is now reasonably certain that there will be a series of boom-mounted, scalar-quality, vector-magnetic experiments on the Block 5 DMSP satellites, which will span the time frame from 1995 through 2005. Two of these satellites will be maintained in orthogonal, sun-synchronous polar orbits at all times. Follow-on Block 6 satellites with full vector capability are also being considered to cover the 2005 through 2015 time frame. Second, we note that the Johns Hopkins Applied Physics Laboratory's Upper Atmosphere Research Satellite (UARS) was launched in September 1991, while the Swedish satellite, Freja, was launched in September 1992. Attempts are being made to secure vector data from these satellites, although the data reduction may be somewhat lengthy since neither data set is of Magsat quality. A Danish satellite project called Oersted, which is intended to be of Magsat quality, had been planned for launch in the latter part of the 1990's. This project received funding from the Danish government in 1993 and is now proceeding beyond the planning stages to an eventual launch in cooperation with NASA in the 1996 time frame.

The current prospects for securing geomagnetic survey data to support World Magnetic Modeling for the next 20 years or so are summarized in Figure 19. It seems from this summary that there will be, as this century closes and the new century begins, a continuous data flow which will guarantee the availability of high-quality Main field and Secular Variation models for the foreseeable future. These data will provide long-term, continuous detailed mapping of the earth's magnetic field which in turn will provide for the first time a means to extend our knowledge of the earth's deep interior through close monitoring of its magnetic secular behavior. Thereby, the future seems bright for the improved predictive capability of our models and for the wide range of applications they support.

WORLD MAGNETIC MODEL DATA ACQUISITION PROFILE

SUPPORTS MAIN FIELD AND SECULAR VARIATION MODELS

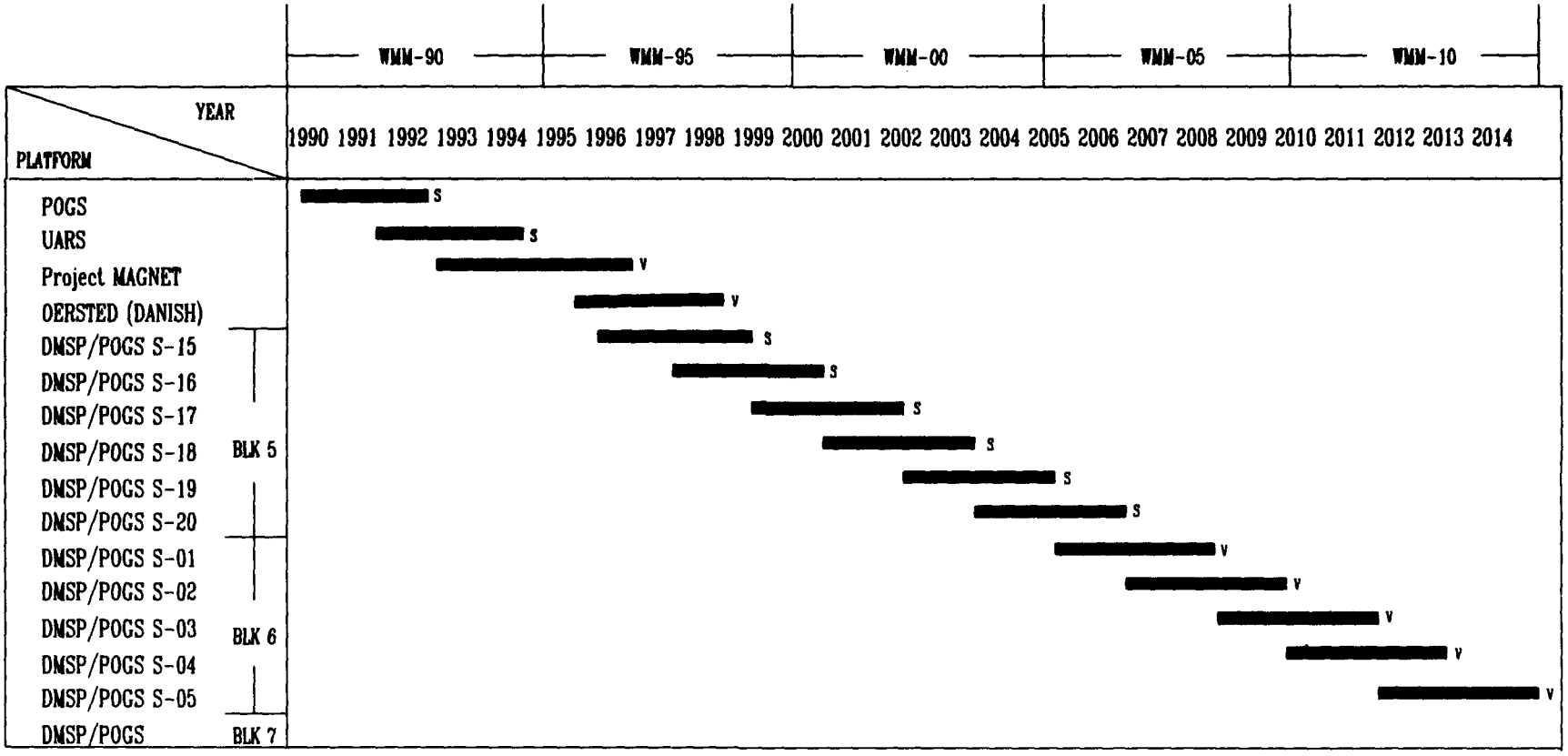

S = VECTOR MAGNETOMETER USED IN SCALAR MODE DUE TO POOR ATTITUDE DETERMINATION OF THE INSTRUMENT

V = VECTOR MAGNETOMETER USED IN VECTOR MODE DUE TO GOOD ATTITUDE DETERMINATION AND INFLIGHT CALIBRATION

Figure 19. Geomagnetic Data Acquisition Profile 1990 - 2015

REFERENCES

Campbell, W. H.; The Regular Geomagnetic Field Variations During Quiet Solar Conditions, in **GEOMAGNETISM**, Vol. 3, Chapter 6, Edited by J. A. Jacobs, Academic Press, San Diego, CA (1989)

Campbell, W. H.; Geomagnetic Storms, Lognormal Distributions, and the Dst Ring-Current Myth, *Journal of Geophysical Research* (in Press)

Cappellari, J. O., C. E. Velez, and A. J. Fuchs; Mathematical Theory of the Goddard Trajectory Determination System, *Technical Report X-582-76-77*, NASA/GSFC (1976)

Chomay, D. J.; Operations Handbook for DMSP/SSM Magnetometer, NASA/GSFC Laboratory for Extraterrestrial Physics (1987)

Goddard Space Flight Center; Spacecraft Magnetic Test Facility (Attitude Control Test Facility) SMTF (ACTF), *Technical Report No. X-754-83-9*, NASA (1984)

IAGA Working Group V-8; IGRF, 1991 Revision, *EOS Transactions*, Vol. 73, No. 16, American Geophysical Union (1992)

O'Toole, J. W.; Celest Computer Program for Computing Satellite Orbits, *Technical Report - 3565*, Naval Surface Weapons Center/Dahlgren Laboratory (1976)

Moritz, H. and I. I. Mueller; **EARTH ROTATION: Theory and Observation**, Frederick Ungar Publishing Co., New York (1987)

Mueller, I. I. and H. Eichhorn; **SPHERICAL and PRACTICAL ASTRONOMY: as Applied to Geodesy**, Frederick Ungar Publishing Co., New York (1977)

Quinn, J. M., R. J. Coleman, M. R. Peck, and S. E. Lauber; The Joint US/UK 1990 Epoch World Magnetic Model, *Technical Report No. 304*, Naval Oceanographic Office (1991)

Stern D. P., R. A. Langel, and G. D. Mead; Backus Effect Observed by Magsat, *Geophysical Research Letters Vol. 7*, pp. 941-944 (1980)

DISTRIBUTION LIST

NAVY	
Chief of Naval Operations	5
Chief of Naval Research	2
David Taylor Naval Ship Research and Development Center	2
Dept. of the Navy, Submarine Combat and Weapons Systems	1
Mine Countermeasure Group Two	1
Mine Warfare Command	1
Marine Corps Research, Development and Acquisitions Command	1
Naval Air Systems Command	1
Naval Air Test Center	2
Naval Air Warfare Center	4
Naval Avionics Center	1
Naval Coastal Systems Center	2
Naval Command Control and Ocean Surveillance Center	2
Naval Oceanographic Office N342, N4312	150
Naval Oceanographic Office N2, N25CL, N25CP, N5	4
Naval Oceanography Command	3
Naval Oceanography Command Detachments (All)	50
Naval Ocean Systems Center	3
Naval Postgraduate School	3
Naval Research Laboratory, Washington DC	6
Naval Research Laboratory Detachment SSC	6
Naval Sea Systems Command	3
Naval Surface Warfare Center, White Oak	4
Naval Surface Weapons Center, Dahlgren	3
Naval Surface Weapons Laboratory Detachment, White Oak	3
Naval Technical Intelligence Center	1
Naval Undersea Warfare Center Detachment, San Diego	1
Naval Underwater Systems Center Detachment, New London Laboratory	1
Naval Underwater Systems Center Detachment, Newport Laboratory	1
Naval Underwater Warfare Center	3
Naval Weapons Center	1
Office of Advanced Technology	2
Office of Naval Research, Washington DC	3
Office of Naval Research Detachment SSC	2
Office of Naval Technology	1
Space and Naval Warfare Systems Command PMW-182, PMW-185	2
USMC 3rd. R.P.V. Experimental Brigade	2
U. S. Naval Academy (Nimitz Library)	1
AIR FORCE	
Air Force Institute of Technology	1
Air Force Office of Scientific Research	1

Pacific Missile Test Center	3
Rome Research Laboratory	2
U. S. Air Force Academy (Technical Library)	1
USAF Air Warfare Center	1
USAF Hq., Electronics Systems Division	1
USAF Phillips Laboratory, AFGL	2
USAF Phillips Laboratory, Kirkland AFB	1
USAF Weapons and Tactics Center	1
ARMY	
Harry Diamond Laboratory (Technical Library)	1
U. S. Army Combat Systems Test Activity	2
U. S. Army Research Laboratory	3
U. S. Military Academy (Technical Library)	1
DOD	
DARPA, Submarine Technology Program	1
DARPA, Nuclear Monitoring Program	1
Defense Mapping Agency, Aerospace Center	4
Defense Mapping Agency, GPS-NAVSTAR JPO	1
Defense Mapping Agency Headquarters	4
Defense Mapping Agency, Hydrographic and Topographic Center	3
Defense Mapping Agency, Systems Center	3
Defense Mapping School	2
Defense Technical Information Center	2
Los Alamos National Laboratory	2
National Security Agency	1
Sandia National Laboratory (Technical Library)	1
NON-DOD	
Australian Geological Survey	1
British Geological Survey	2
Bedford Institute of Oceanography (Technical Library)	1
Canadian Defence Research Establishment Pacific	2
Colorado School of Mines, Center for Potential Field Studies	2
Geological Survey of Canada, Geophysics Division	3
Geological Survey of Canada, Atlantic Geoscience Centre	3
Geological Survey of Canada, Pacific Geoscience Centre	3
Geothe Universitat, Institute Fur Meteorologie und Geophysik	3
Hatfield Marine Science Center	3
Istituto Nazionale Di Geofisica	1
IZMIRAN	2
Institut de Physique du Globe de Paris	2
Johns Hopkins University, Applied Physics Laboratory	1
Lawrence Livermore Laboratory (Technical Library)	1
McGill University, Dept. of Earth and Planetary Sciences	1

NASA, Geodynamics Branch	5
NOAA, NGDC	3
NOAA, Pacific Marine Environment Laboratory	2
Oregon State University, College of Oceanography	1
Purdue University, Dept. of Earth and Atmospheric Sciences	1
Raytheon Corporation	2
Royal Australian Navy, Maritime Hq.	2
SACLANT ASW Research Centre	2
Scripps Institution of Oceanography	2
Stanford University, Dept. of Geological Sciences	1
Tracor, Incorporated	3
U. S. Geological Survey, Denver	5
U. S. Geological Survey, Menlo Park	2
University of Cantebury, Dept. of Geology	1
University of Michigan, Dept. of Geophysics	1
University of Rhode Island, Graduate School of Oceanography	1
University of Sydney, School of Mathematics and Statistics	1
University of Toronto, Dept. of Physics, Geophysics Laboratory	1
University of Washington, School of Oceanography	2
Woods Hole Oceanographic Institution	2